The Development of Components for an *In-situ* Mass Spectrometer

by

Richard Camili

B.A., Biology (1996)

Cheyney University

Submitted to the Department of Civil and Environmental Engineering
In Partial Fulfillment of the Requirements for the Degree of
Master of Science in Civil and Environmental Engineering

at the

Massachusetts Institute of Technology

May 2000
[June 2000]

Signature of Author.....
Department of Civil and Environmental Engineering
May 5, 2000

Certified by .....
Harold F. Hemond
Professor of Civil and Environmental Engineering.
Thesis Supervisor

Accepted by.....
Daniele Veneziano
Chairman, Departmental Committee on Graduate Studies

THE DEVELOPMENT OF COMPONENTS FOR AN *IN-SITU* MASS SPECTROMETER

by

RICHARD CAMILI

Submitted to the Department of Civil and Environmental Engineering
on May 5, 2000 in partial fulfillment of the
requirements for the Degree of Master of Science in
Civil and Environmental Engineering

ABSTRACT

Many aspects of inquiry in marine systems require knowledge of the identity and concentrations of dissolved gases and volatile substances in the water column. Data characterizing variability in dissolved gases in the marine environment provide insight into many poorly understood environmental processes. The goal of this research is to develop components for a low-power, automated instrument capable of real-time, *in-situ*, measurement of dissolved gases, thereby enabling high-resolution temporal and spatial mapping of dissolved gas distributions on local to basin scales. Specifically, these components are for a membrane inlet mass spectrometer (MIMS) designed to operate autonomously either on board a Sea Grant Odyssey class autonomous underwater vehicle (AUV), as a moored instrument package, or on a variety of other platforms.

Over the past decade the call for more advanced *in-situ* sensing systems for continuous and real-time measurements of dissolved chemicals has grown (Wakeham 1992; Takahashi, Wunsch et al. 1993). Conventional measurement of dissolved gases at depth requires that water samples be collected and then relayed to a laboratory for analysis, a process that is slow and labor-intensive, and requires precautions against chemical and physical changes occurring during collection and transport *(i.e. degassing, photochemistry, microbial metabolism)*. Existing *in-situ* devices (*e.g.* DO probes) are commonly limited to detecting one or a few gas species (Takahashi, Wunsch et al. 1993), with separate sensors required for each specie and sensitivities of typically about 1 ppm. Continuous sampling techniques (*e.g.* Weiss equilibrator) are generally limited to shipboard use and modest sampling depths, and have gas specie dependent equilibration constants from minutes to hours (Conrad and Seiler 1988; Park 1995; Bates, Kelly et al. 1996; Johnson 1999). By comparison, a MIMS system has the potential to rapidly and autonomously measure dissolved biogenic gases, atmospheric gases, and light hydrocarbons with high resolution. Preliminary calculations and data indicate that the prototype components described here will permit a depth capability of at least 100 meters, response time on the order of seconds and sensitivities for most gases in the tens of ppb range. Thus, the *in-situ*, high sensitivity, multi-species capabilities of the MIMS will fill an important, unmet need of oceanographic and other environmental scientists.

Thesis supervisor: Harold F. Hemond

Title: Professor of Civil and Environmental Engineering

ACKNOWLEDGEMENTS

In Canto II of *The Inferno*, Dante wrote of his hesitancy to follow Virgil into hell. Like Dante, I too had misgivings when I first arrived at 77 Massachusetts Avenue. However, in the nearly 700 years since his writing, MIT has greatly expanded its real estate. There are now circles of hell reserved for those who have committed sins un-thought of in Dante's time --sins of technological impiety. Transgressions in the name of attempting to create fractions of a Torr of nothingness, sculpting incorrigible steel, of describing μvolts in bits of eight; I list but a few. There, among the smoldering cutting tools and moribund integrated circuits, the chaos of Murphy's law set upon me. It is within these circles that I have labored for what, according to friends, has been eternity.

As Dante had the poet Virgil to guide him with reason through the levels, I have had the indispensable guidance of my poet-advisor, Professor Hemond. Through his instruction I have learned what would have taken decades if left to my own devices. With Beatrice's divine protection Dante knew no peril, so too the aegis of loving family and friends have strengthened and protected me. My mother's prayers of compassion are garments I have worn from birth, safeguarding me from life's inclemencies. Saint Lucia's divine light is a fire ignited by the Reddy family, making my path clear. Contemplative life, a gift granted by my siblings and friends. Iván, the wise old Boriqua revolutionary. Luis "Tanzania Jones", bull riding archaeologist and counterpoint to Babylon. Julia, champion of idealism. Dr. Amin Mery, forever proving that laughter is the best medicine. Chris Merkey, undisputed mundo del mondo and creator of VW restoration psychotherapy. Dr. Jenny Jay (the original veggie Doc) and Anand "imperial pint drinking" Patel, two genuine humanitarians and first-rate crewmates. My intellectual wingmen, three modern day musketeers: Luisto Perez-Prado, Enrique Vivoni, and Carlos Rinaldi. The Wall Street wizards, J. Alain & Tina Ferry. Garrett Cradduck and Tony Chang, the prime number hunting-combinatorialist pool sharks.

Along with these individuals, the *deus ex machina* within the Institute and elsewhere have played a vital sustaining role in my endeavors. Without the generous support of the National Science Foundation, the Alfred E. Sloan Foundation, the Ralph M. Parsons Foundation, and the William E. Leonhard Endowment, my graduate education would probably have remained just an aspiration. Likewise, the stalwart advocacy of the Graduate Education Office has allowed me to transcend otherwise insurmountable obstacles. Discussions, insights, and general laboratory assistance from fellow students, faculty, and staff of the Parsons laboratory, especially Sheila Frankel, Vicki Murphy, and members of the Hemond research group, have proven an invaluable resource.

Thank you, everyone.

As flowerlets drooped and puckered in the night
turn up to the returning sun and spread
their petals wide on his new warmth and light-
just so my wilted spirits rose again
and such a heat of zeal surged through my veins
that I was born anew. Thus I began:

Dante Alighieri, *The Inferno*

TABLE OF CONTENTS

TABLE OF FIGURES

TABLE OF EQUATIONS

Chapter 1

INTRODUCTION

The objective of this project is to develop components for a prototype instrument that will combine the analytical power of mass spectrometry, the advantages of *in-situ* analysis, and the range, autonomy, and cost effectiveness of a modern, low cost, autonomous underwater vehicle. Such an instrument will be invaluable for helping understand numerous processes in coastal and deep ocean systems (and freshwater systems as well). A mass spectrometer is chosen for *in-situ* dissolved gas analysis because a) a mass spectrometer is a universal detector, b) a mass spectrometer can detect chemicals at low concentrations, c) mass spectra can be quickly processed to yield chemical identities and concentrations in mixtures of several compounds and d) mass spectrometers can operate without reagents or exhaust. These characteristics make mass spectrometers well suited for real-time *in-situ* analysis of dissolved gases. A membrane inlet mass spectrometer is chosen for simplicity as well as selectivity for the gases of interest relative to water.

Although several field portable mass spectrometers are now commercially available (Baykut and Franzen 1994), none possess the requisite characteristics for operation on an AUV. Therefore, this project was undertaken to develop specialized components that will allow for completely autonomous underwater operation of a mass spectrometer. Engineering obstacles to be overcome include size constraints, limited power budget, and resistance to high hydrostatic pressures. Much of the AUV-MIMS

development draws upon a successfully field tested backpack portable mass spectrometer built by Professor Hemond of MIT (Hemond 1991). As of this writing, many of the MIMS components have been fabricated and tested, including the vacuum envelope, membrane inlet, digital mass selection controller, and data acquisition system. Additional items, such as a permanent magnet and an instrument mounting frame have been designed but await fabrication. Finally, an embedded computer & power supplies, and an emission regulator are required for instrument completion.

When completed, the membrane inlet mass spectrometer (MIMS) components will enable autonomous underwater operation on a mooring or fixed platform. Value of the MIMS instrument will be further increased through the ability to use an autonomous underwater vehicle (AUV) as a platform. The AUV allows for data collection in environments that are not easily accessible, while providing continuous chemical mapping. The AUV also provides the added advantages of high resolution, continuous, temporal or spatial data collection - all difficult to achieve by manual sampling, followed by off-site analysis or even shipboard chemical analysis. Additionally, unlike remotely operated vehicles (ROVs), AUVs do not require a tether with a human operator and can thus move faster than ROVs as well as operate during hazardous weather conditions or in areas inaccessible to a ROV support ship.

The Odyssey class AUV is a low cost, fully autonomous submarine developed by MIT Sea Grant (Figure 1.0-1), which is capable of carrying a sensory payload within one of its two internally housed pressure spheres. This class of AUVs has an endurance of 12 hours at 5 km/hr without recharging, displaces approximately 165 kilograms, and can

Figure 1.0-1: Odyssey class AUV

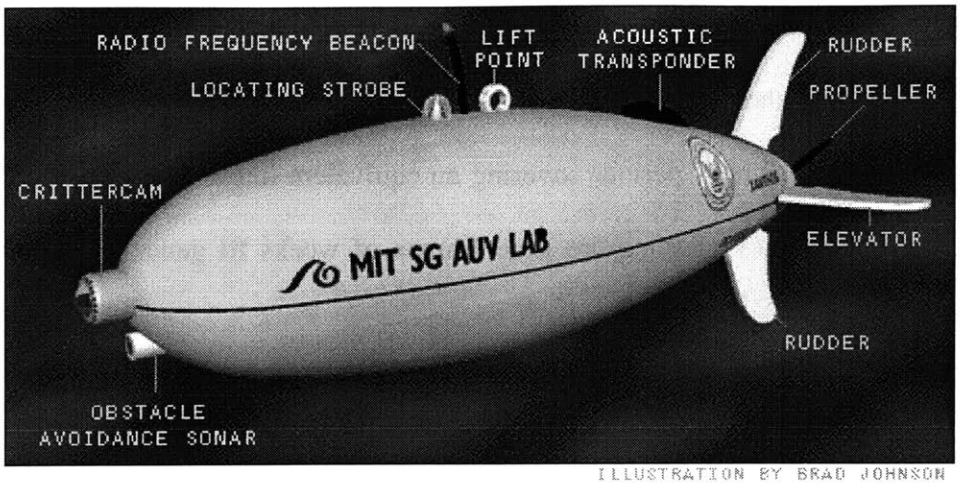

dive to depths of 6,000 meters (Bellingham, Goudey et al. 1992). Odysseys have been successfully demonstrated in several field trials, including missions in Antarctica, New Zealand's Kaikura Canyon (Bellingham 1997), and Vancouver Island's Haro Strait (Bellingham, Moran et al. 1996). Given the Odyssey performance characteristics, the MIMS will rapidly generate high-resolution data for mapping temporal and spatial distribution of dissolved gasses on local to basin scales. Calculations indicate that the mass spectrometer will be able to detect dissolved biogenic gases, atmospheric gases, and light hydrocarbons with masses from 2 to 150 AMU, with detection limits as low as 10 ppb. and response times on the order of seconds. The dynamic range of the data acquisition system will allow for measurements of concentrations up to 1 part per thousand. By comparison, most existing *in-situ* dissolved gas measuring devices can only detect a single type of gas with a detection limit of only about 1 ppm and response times as long as minutes. Pressure testing and calculations indicate that the current prototype can withstand depths to 100 meters; further development should allow for greatly increased depth capabilities. The prototype will be able to operate throughout the

entire water column of many freshwater bodies, as well as many marine coastal areas such as Chesapeake Bay and Cape Cod Bay. Odyssey endurance, coupled with the MIMS sampling frequency, should make it possible to generate a total of approximately 43,000 data points during a 12 hour period, covering an equivalent linear distance of 60 km. In contrast, current technologies require time frames of weeks to generate an equivalent amount of data.

Chapter 2

APPLICATIONS

Potential applications for this instrument include geochemical, ecological, hydrological, and chemical fate analyses. Geochemical applications may include marine mapping of dissolved gases from hydrothermal vents and ocean floor seeps. Dissolved marine gases can vary widely both spatially and temporally (Conrad and Seiler 1988; Tilbrook and Karl 1995; Tsurushima, Watanabe et al. 1996; Sansone, Rust et al. 1998). Investigations of methane seeps are valuable for offshore oil exploration and global climatological research. This hydrocarbon is often observed in increased concentrations in areas of freshwater inputs (Scranton and McShane 1991), anaerobic zones of bottom sediments (Martens 1976), oil and gas deposits, destruction of crystallohydrates, and emission along fractures in the earth's crust (Alper 1990; Dafner, Obzhirov et al. 1998).

Deepsea hydrothermal vents have been the subject of increased interest from global climatological and biological perspectives. The reduced gases from these vents are known to give rise to entire chemosynthetic ecosystems (Alper 1990) which oxidize methane or sulfide to produce energy. Sources such as anhydrite chimneys of the North Fiji Basin and hydrothermal vents on the East Pacific Rise have been shown to emit gases in concentrations exceeding 14.5 parts per thousand of carbon dioxide, 1.4 parts per thousand of hydrogen gas, 49 ppm of methane, and approximately 937 ppb of helium (Welhan and Craig 1983; Ishibashi, Wakita et al. 1994).[1] These concentrations would be

[1] For consistency, concentrations are expressed as a mass fraction

easily detectable using the MIMS instrument, enabling chemical concentration surveys of known sites and identification of previously unknown geologic sources.

Hydrologic research often utilizes dissolved gas data to determine source and age of waters. Concentrations of oxygen, nitrogen, carbon dioxide, and methane can provide valuable clues to origins and inflow rates of ground and surface waters into estuaries and coastal areas (Bussmann and Suess 1998). The ability of the MIMS to identify and quantify the distribution of biogenic gases in a water column is also useful for many aspects of ecological research. As an example, the N_2/Ar ratio is accurately measurable by membrane inlet mass spectrometry, and is potentially valuable in assessing denitrification. AUV/MIMS systems could also be used to unobtrusively monitor water quality, especially from urban runoff, shipping lanes, and point sources of pollution such as sewage outfalls. Another example is the ability to accurately measure O_2 at sub- ppm levels, where even the best polarographic electrodes do not always reliably distinguish small but ecologically significant concentrations of O_2 from "zero" levels of O_2.

Mapping of marine oil spills for impact assessment and cleanup is yet another potential MIMS application. Oil spill surveillance relies almost exclusively on remote sensing such as infrared, ultraviolet, and radar imaging from satellites and planes (Fingas and Brown 1997). These approaches are only suitable for detecting surface slicks, and are unable to detect dissolved petroleum fractions at depth. Oil spill assessment based on surface slick as well as sub-surface data is important when DNAPL or water-soluble fractions are present and when wave induced mixing is a factor. For instance, approximately 77% of the 825,000 gallons of petroleum from the North Cape oil spill was dispersed into the water column (Lehr, Galt et al. 1996). Estimates of this spill's size, based upon oil-slick area, underestimated the magnitude of the disaster, thus contributing

to an ill-prepared cleanup response. In an occurrence such as this, MIMS would be unable to detect many of the heavier hydrocarbons (M/Z > 150) such as poly-aromatic hydrocarbons. However, it could easily detect lighter volatile hydrocarbons, including butane. Future sample introduction schemes may allow for measurement of larger hydrocarbons and their fragments, such as the butane cation ($C_4H_9^+$), which is a major ion in aliphatic compounds and is commonly used to calculate total petroleum hydrocarbons (Reddy and Quinn 1999).

Chapter 3

INSTRUMENT DESIGN

The MIMS instrument is designed to be self-contained, operating within a 17 inch Benthos pressure sphere. The pressure sphere functions to protect instrument components from ambient water, which can reach pressures up to 850 atmospheres. The instrument can be divided into 3 major component groups: the vacuum system, the analyzer, and the electronics system (Figure 3.0-1). The vacuum system consists of a membrane inlet apparatus, inlet tube, vacuum envelope, and ion pump. The inlet apparatus and inlet tube are used to exclude water, while allowing for adequate analyte gas inflow to the analyzer. The ion pump cooperatively maintains a low-pressure environment, permitting analyte gas ion acceleration and detection under free molecular flow conditions within the vacuum envelope. The analyzer component group, which is mostly contained within the vacuum envelope, includes the ion source, cycloidal mass selector, and Faraday cup detector. Also, positioned outside of the vacuum envelope is a permanent magnet, which provides a homogenous B-field for the cycloid. Together, the analyzer components create analyte gas ions, which are then accelerated along predetermined trajectories toward the Faraday cup detector. Bombardment of the Faraday cup detector by these ions generates an ion current that is then sent to the electrometer. The electrometer senses this ion current and transforms it to an amplified voltage signal. This electrometer output voltage is then converted to a digital signal by a controller/data acquisition (DAQ) board and transmitted to an embedded computer which interprets and

Figure 3.0-1: MIMS conceptual design

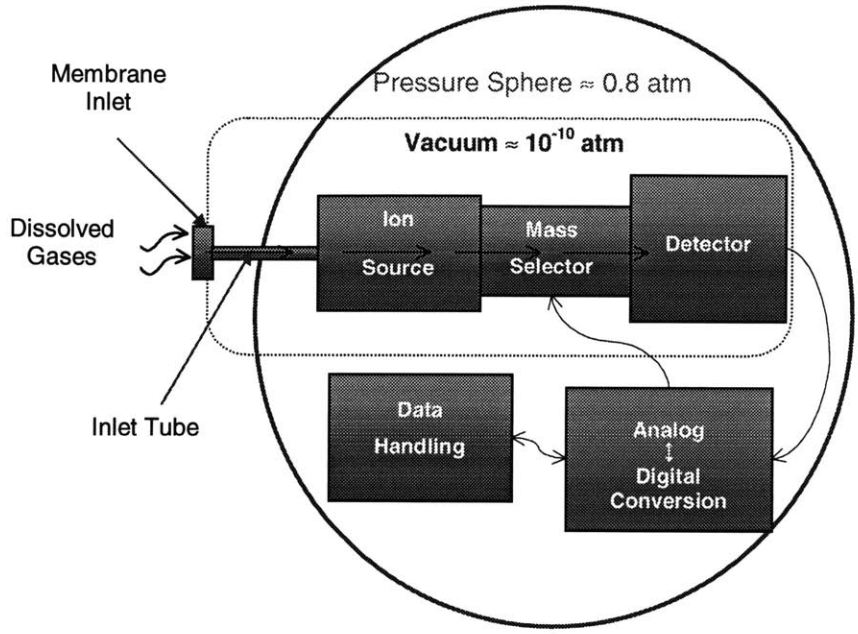

stores this data. After this data handling is completed, the embedded computer calculates the accelerator potential needed to generate an appropriate trajectory for the next mass value. Using the calculated mass value, the DAQ board generates the correct accelerator potential via a high gain amplifier.

Design and construction of the MIMS package requires analysis and optimization of the three component groups. The remainder of this section seeks to provide the reader with an overview of relevant design issues. Therefore, in an attempt to provide an intuitive format, factors affecting instrument operation are divided into conceptual sub-sections. Each sub-section introduces, in a stepwise fashion, component design & performance issues contributing to overall instrument functioning. They are as follows:

- Vacuum system
  - Maximum depth capability of inlet apparatus
  - Maintenance of free molecular flow environment
- Analyzer
  - Cycloid performance characteristics
  - Compact, low power design
- Sensitivity
  - Minimum detectable concentrations of dissolved gases
- Response time
  - Diffusion of gases across unstirred water layer
  - Diffusion of gases across inlet membrane
  - Inlet tube conductance & residence time
  - Electrometer response time
- Computerized control
  - Automated mass selection & peak height detection
  - Digital accuracy
  - Sampling frequency
- Data handling
  - Storage & transfer
  - Spectrum separation
- Packaging
  - Layout
  - Housing & mounting frame
- Calibration

3.1 Vacuum System

The vacuum system, which houses the cycloid, is comprised of various components including a membrane inlet, inlet tube, vacuum envelope, and ion pump. Space limitations have required that the vacuum system have a compact geometry, yet allow for adequate gas conductance rates. The vacuum envelope is constructed of welded #304 stainless steel and contains the ion source, mass selector, and detector. Roughly the size of the soft drink can (Figure 3.1-1), it was designed to be small enough to fit within the pressure sphere, yet permit satisfactory conductance of excess gases into the ion pump.

Sample gases first diffuse from the water column in through the membrane inlet, then move down the inlet tube into the vacuum envelope. Once gas molecules enter the

vacuum envelope, they are ionized and then accelerated through the mass selector, finally impacting the Faraday cup detector.

Figure 3.1-1: Vacuum system

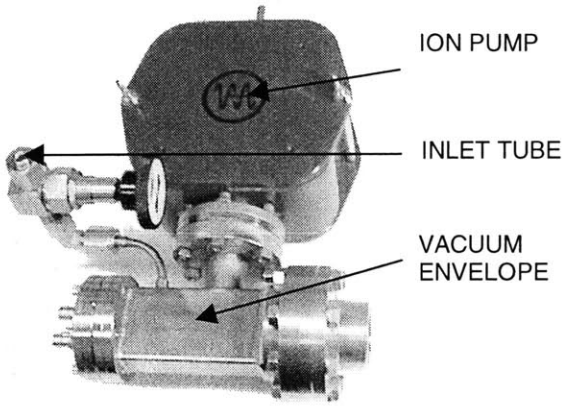

3.2 Inlet apparatus

The inlet system, which is to be positioned outside of the pressure sphere, is designed to exclude water, while allowing for adequate analyte inflow by means of a hydrophobic membrane capable of maintaining an internal vacuum of 10^{-8} Torr. A physical challenge for marine deployment of the membrane inlet system is to withstand hydrostatic pressures up to 580 atmospheres. The inlet consists of an annular stainless steel cap threaded onto a stainless steel inlet body. Between the inlet body and cap are a stainless steel and a Teflon washer in series, which secure a 1mil thick polymer membrane over a stainless steel micro-etched backing plate (Figure 3.2-1) (see also APPENDIX C: Inlet apparatus Ortho cut away view, pp. 89). Possible failure modes include backing plate collapse caused by excessive hydrostatic pressure, membrane rupture caused by excessive hydrostatic pressure, as well as excessive water vapor influx across an intact membrane due to a thermally or chemically induced increase in membrane permeability. In addition to the problems associated with a catastrophic failure

of the inlet, significant water vapor input can cause a reduction in signal response through the collision of water molecules with analyte ions. A variety of polymers have been investigated for use as a hydrophobic semi permeable membrane (Richardson 1988; Ernst 1994), low-density polyethylene (ρ = 0.914) having the most desirable strength and permeability qualities.

Figure 3.2-1: Inlet apparatus

Determination of the maximum operational depth limit of the inlet system requires strength calculations (hydrostatic pressure loading) for the stainless steel backing plate and polymer membrane. The membrane can be modeled as an edge held, uniformly loaded circular diaphragm of uniform thickness, without flexural stiffness (Roark and Young 1975). To calculate maximum membrane loading, membrane vertical deflection at the center is first determined (Equation 1),

Equation 1:
$$\frac{\tau[psi]\,a[in]^2}{E[psi]\,t[in]^2} = K_3\frac{y[in]}{t[in]} + K_4\left(\frac{y[in]}{t[in]}\right)^2$$

where τ is the membrane's tensile strength (psi.), a is radius (in.), E is modulus of elasticity (psi.), K_1-K_4 are proportionality constants, q is maximum load (psi.), t is membrane thickness (in.), and *y* is vertical deflection (in.). The deflection term is then used to solve for maximum loading *(*Equation 2*).*

Equation 2:
$$q[psi] = \frac{E[psi]\,t[in]^4\left(K_1\frac{y[in]}{t[in]} + K_2\left(\frac{y[in]}{t[in]}\right)^3\right)}{a[in]^4}$$

Three general ways of supporting the backing plate are possible: simple, guided, and edge held supports (Figure 3.2-2). A simply supported plate allows for flexing of the plate at its edges as well as movement of the plate with respect to the support as the plate deforms under load; thus, only making use of the unsupported area's rigidity. By contrast, the guided support does not allow for flexing of the plate at its edges, but does allow the plate to move with respect to the support; thereby utilizing the unsupported area's rigidity and the supported area's rigidity leveraged against the support edge. The edge held regime does not allow for flexing of the plate at its edges nor the movement of the plate with respect to the support; thus resulting in a "tensioned" support of the plate. However, a precise edge condition is unlikely, and a truly fixed edge is especially difficult to attain. Even a small horizontal force at the line of contact may appreciably reduce the stress and deflection in a simply supported plate; however, a very slight yielding at fixed edges will

greatly relieve the stresses there while increasing the deflection and center stresses (Roark and Young 1975).

Figure 3.2-2: Types of supports

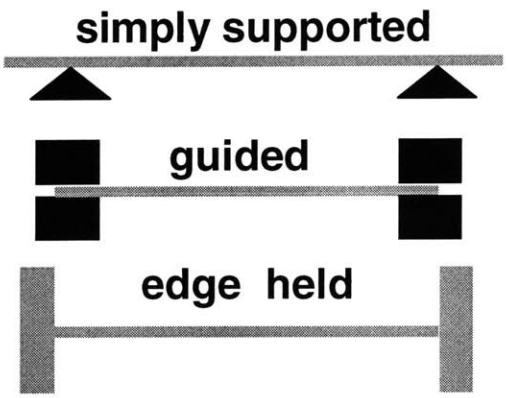

The empirical equation used to describe yield strength of a circular, uniformly loaded, simple support (Equation 3) is nearly identical to the equation used to describe the yield strength of an edge held plate regime (Equation 4) (Roark and Young 1975).

Equation 3: $$q[psi] = \frac{\tau[psi] \times t[in]^2 \times 16}{6 \times a[in]^2 \times (3 + \nu[unitless])}$$

Equation 4: $$q[psi] = \frac{\tau[psi] \times t[in]^2 \times 16}{6 \times a[in]^2 \times (1 + \nu[unitless])}$$

In both these equations ν is the material's Poisson's ratio (unitless), τ is tensile strength (psi.), a is the disk radius (in.), q is the maximum loading (psi.), and t is thickness (in.). The difference between the two equations is only the value of the Poisson's ratio addend. Given #304 annealed stainless steel's characteristic Poisson's ratio of .28, a backing plate

utilizing an edge held support is stronger than a simple support by a factor of approximately 2.5.

The inlet system uses a backing plate support that can be approximated as a quasi-simple support. To avoid over estimation of the plate strength, an equation based on the simple support equation is used which has been augmented with an additional term. This term, V, is included to account for decreased strength caused by the micro-etched holes, and is expressed as the backing plate's surface area to hole void ratio. Using this derivation, a lower limit of the backing plate yield strength can be calculated (Equation 5).

Equation 5:
$$q[psi] = \frac{\tau[psi] \times t[in]^2 \times 16 \times (1 - V[unitless])}{6 \times a[in]^2 \times (3 + \nu[unitless])}$$

Once the maximum loading of the membrane and plate have been calculated, a maximum depth rating for each can easily be found. Based on these calculations, the backing plate has a predicted maximum depth rating of approximately 95 meters, while the membrane is predicted to have a maximum depth rating of 118 meters. Although the calculated yield strength of the backing plate is 18% less than the membrane, the support method used for the backing plate is likely to be a hybrid of the simple, guided, and fixed supports. Therefore, the backing plate may actually be stronger than the membrane. Preliminary tests show that the inlet system is capable of withstanding hydrostatic pressure to an equivalent of at least 74 meters depth. Further, destructive testing is needed to ascertain the absolute depth capability of the inlet system.

Modifications such as usage of an edge held backing plate, increase backing plate thickness, as well as additional backing plate support using a honeycomb type

reinforcement (Figure 3.2-3), increasing membrane thickness and decreasing the unsupported membrane radius may dramatically increase inlet system depth capability (**Figure 3.2-4**) (see also APPENDIX D: Tables of inlet backing plate and membrane depth limits using various design specifications, pp. 101-102).

Figure 3.2-3: Backing plate depth rating

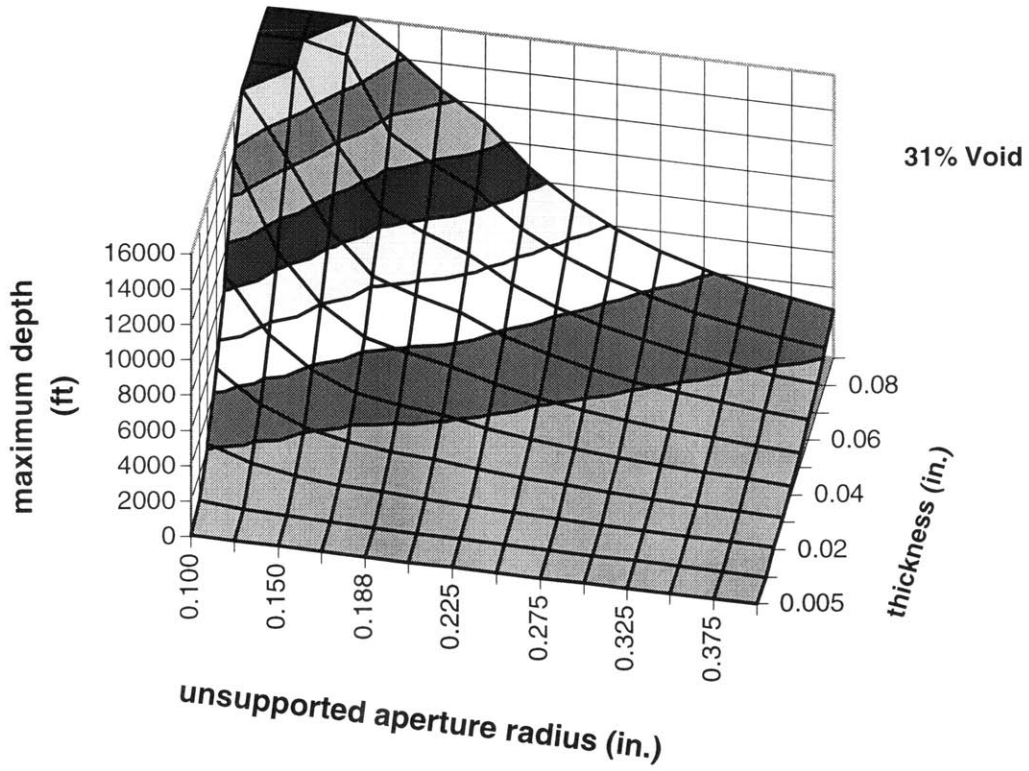

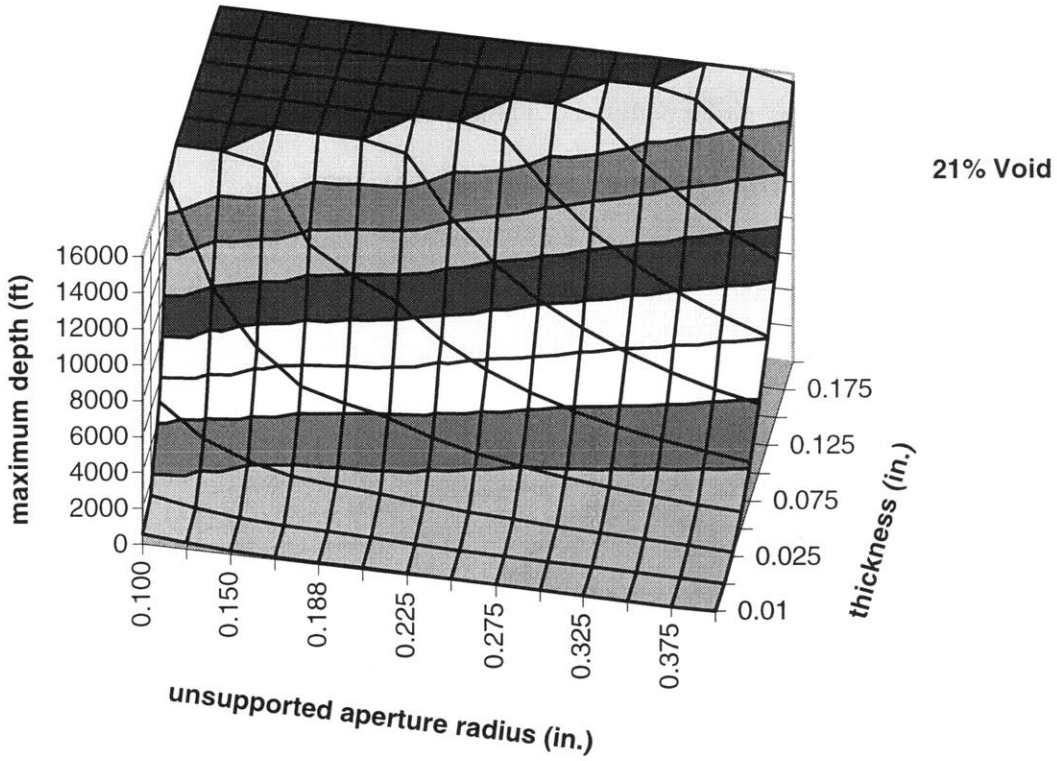

Figure 3.2-4: Membrane depth rating

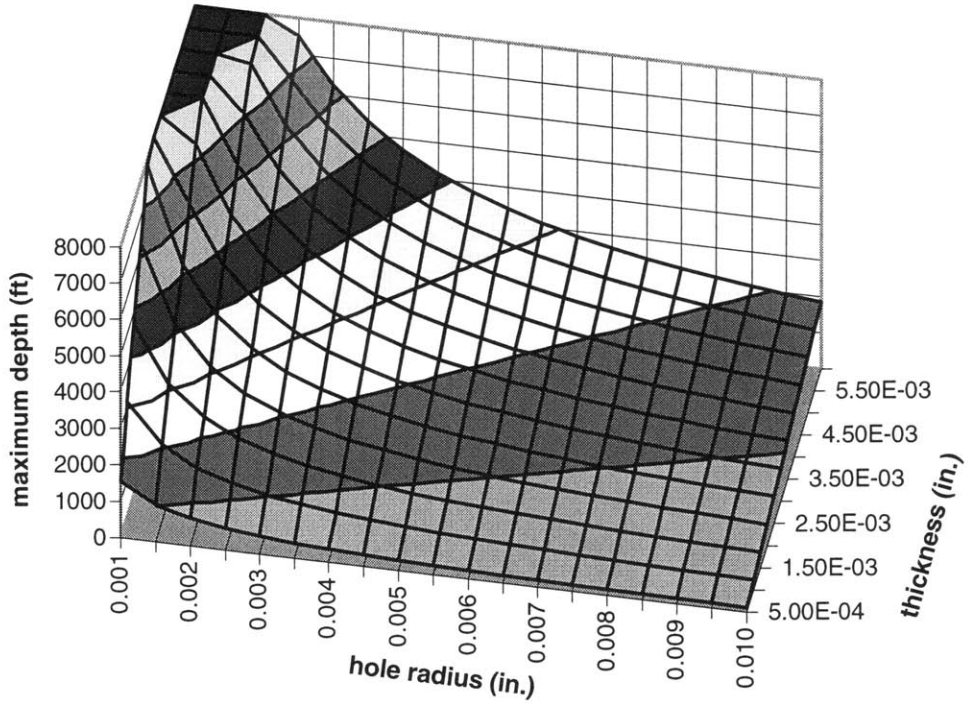

3.2.1 Vacuum envelope

Aquatic samples of dissolved gases contain water in concentrations of approximately 55 moles per liter, while dissolved gases of interest are nominally of micro-molar to nano-molar concentrations. Because water vapor is the most abundant gas to enter the vacuum system, far in excess of all other gas species combined, the steady state pressure within the vacuum envelope can be estimated based on water vapor influx alone. Assuming water vapor on the outer surface of the membrane is in equilibrium with the ambient water, water vapor pressure on this surface can be determined. Considering that the volume of the vacuum system remains constant, mass in must equal mass out for vacuum envelope internal pressure to be maintained at steady state (*i.e.* water vapor influx rate equaling vacuum envelope conductance multiplied by internal pressure). To estimate steady state vacuum envelope pressure, the influx rate of water, Q (cm^3 @STP/sec), is first calculated, using the permeability coefficient of water across the membrane, P ([cm^3@STP·cm]/[cm^2·sec·atm]), the membrane surface area, A (cm^2), and the membrane thickness, l (cm); where the internal partial pressure of water, p_2 (atm), is assumed to be negligible and the external membrane water vapor pressure, p_1 (atm), is a function of temperature (Equation 6) (Comyn 1985).

Equation 6:
$$Q\left[\frac{cm^3@STP}{sec}\right] = \frac{P\left[\frac{(cm^3@stp)\cdot cm}{cm^2\cdot sec\cdot atm}\right] A\,[cm^2]}{l[cm]}\left(p_1[atm] - p_2[atm]\right)$$

This influx rate, Q, can then be expressed in L·atm/sec by multiplying by a conversion factor of 10^{-3} L/cm^3. Steady state pressure, p_{ss} (atm), can then be estimated by dividing this flux rate, Q (L·atm/sec), by the vacuum envelope conductance, F (L/sec), (Equation

7) (see also APPENDIX D: Vacuum envelope steady state pressure determination, pp. 100).

Equation 7: $$p_{ss\,[atm]} = \frac{Q\left[\frac{L \cdot atm}{sec}\right]}{F\left[\frac{L}{sec}\right]}$$

For the purpose of estimating gas conductance, the vacuum system can be modeled as a series of long rectangular and circular tubes which are maintained at pressures that allow for free molecular flow (Duschman 1962) (see APPENDIX D: Conductance determinations for vacuum system components, pp. 99).

Water vapor pressure is a function of temperature, consequently the steady state vacuum envelope pressure exhibits a temperature dependence. For the specific parameters of the vacuum envelope, a steady state operating pressure of approximately one order of magnitude less than the operational limit can be expected (Figure 3.2-5). To maintain a pressure of less than 10^{-8} Torr, thereby preventing filament burnout and allowing for adequate mean free path length, excess gas molecules within the vacuum system are sequestered by an eight liter per second diode-type ion pump. However, ion pumps only operate effectively at pressures less than 10^{-4} Torr. Therefore, initial pump down must be performed using a mechanical vacuum pump. To further reduce water vapor associated vacuum envelope pressure and analyzer interference, a $KMnO_4$ desiccant will be utilized within the membrane inlet during operation.

Figure 3.2-5: Steady State Vacuum Envelope pressure

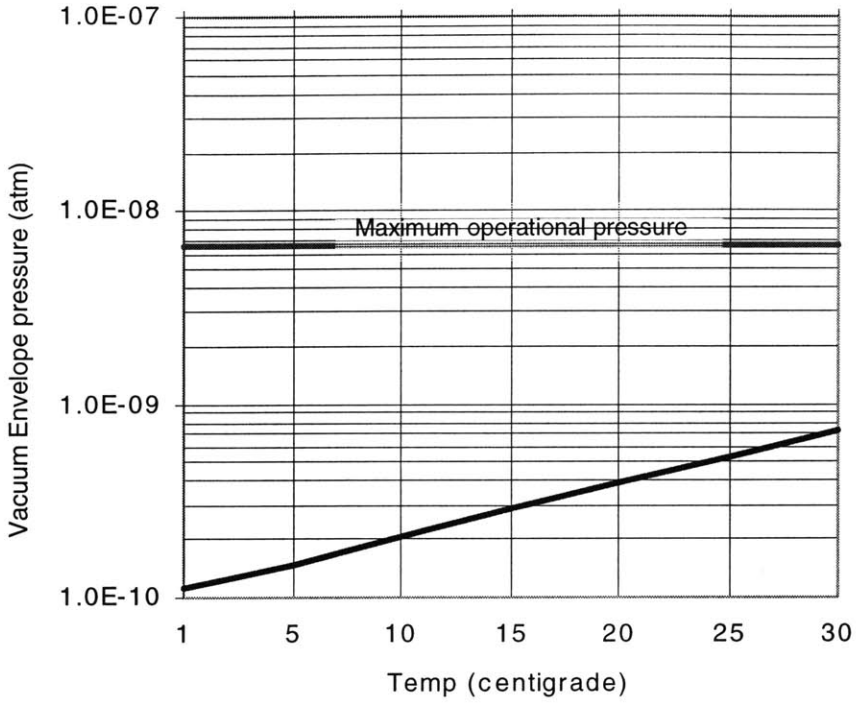

The vacuum envelope is constructed of #304 stainless steel. It consists of a 3 3/8 inch diameter O-ring type flange welded to a 2 x 3 inch (0.049 inch wall thickness) box section tube. The box section is in turn is welded to a 2 ¾ inch conflat flange at its other end. This flange is bolted to a 2 ¾ inch diameter dual BNC feedthrough to allow for connection of the electrometer to the internal Faraday cup. At the center of the box section a 1inch diameter half nipple (2 ¾ inch diameter conflat flange) which provides an outlet port to the ion pump. On the box section, between the half nipple and the feedthrough, is the inlet tube (Figure 3.2-6) (see also APPENDIX C: Vacuum envelope Ortho view & Side view, pp. 91-92). The inlet tube fitting is sized to accept an inflow tube attached to a modified heater plate on the cycloid (see also APPENDIX C: Cycloid heater box Ortho view, pp.90).

Figure 3.2-6: Vacuum Envelope cutaway view

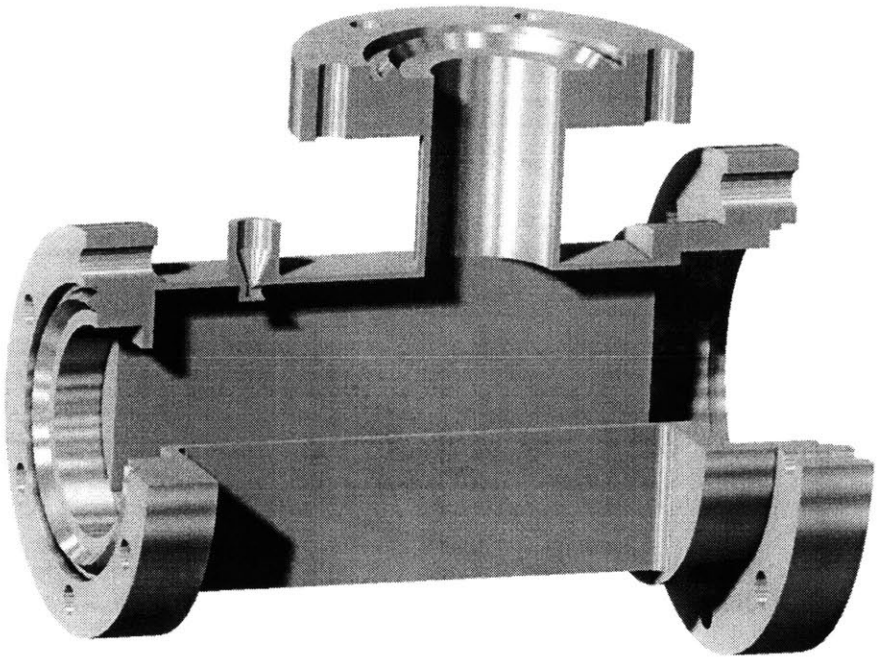

The cycloid is held in place within the vacuum envelope via an eight hole bolt through retaining ring that is secured to the 3/8 inch diameter flange. High vacuum is maintained with a 2.112 inch diameter PTFE Teflon O-ring (0.103 inch thickness) positioned between the cycloid base flange and the 3/8 inch diameter vacuum envelope flange. Teflon was chosen over other materials based on its relative low permeability to gasses, ability to withstand high temperatures that occur during bake-out, and low cost compared to single use gold gaskets.

High vacuum testing of this vacuum envelope, using a Varian 200 L/s oil diffusion pump with a CEC model GIC-100 ionization gauge, has confirmed the ability to maintain pressures as low as 3.5×10^{-8} Torr. Additional testing using a Varian 8 L/s ion pump with a Varian VacIon model 921-0012 pump control unit has demonstrated current

draw as low as 21 μamps at 3.8 kV, corresponding to an approximately equivalent pressure.

3.3 Analyzer

The MIMS employs a modified CEC 21-620 cycloidal type analyzer which uses orthogonally crossed fixed homogenous magnetic and variable homogenous electric fields to impart trochoidal trajectories to sample ions (Figure 3.3-1). Although cycloidal type analyzers are somewhat uncommon, having been largely abandoned by the scientific community three decades ago, this analyzer was chosen over other types of analyzers for several reasons. The cycloidal geometry has the uniquely inherent property of perfect direction and velocity focusing (Bleakney and Hipple 1938), making the analyzer less sensitive to misalignment and vibration. Additionally, because the ion trajectories loop in on themselves a relatively compact flight path, and therefore size, is achievable. The 21-620 cycloidal geometry allows for adequate mass range (2-150 AMU), and a mass resolving power of 100 (Kiser 1965), permitting detection of dissolved biogenic gases, atmospheric gases, light hydrocarbons, and the differentiation of many isotopes.

Figure 3.3-1: Cycloidal ion trajectory

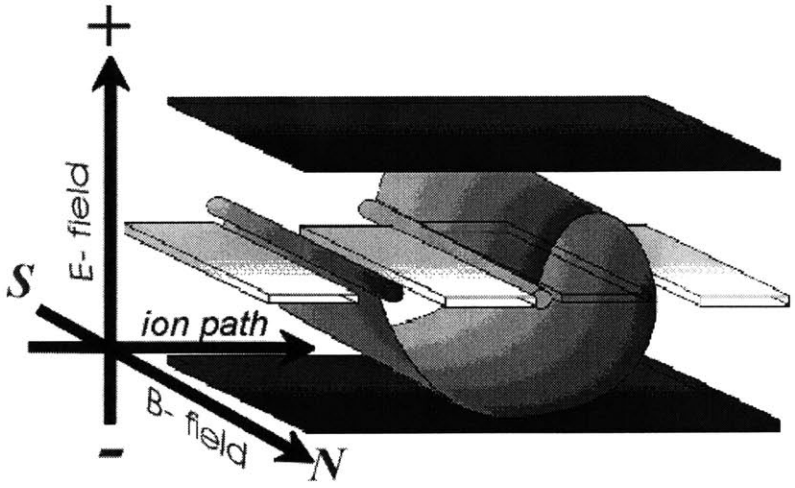

Electric field for the cycloid is produced by a high voltage operational amplifier which supplies a variable potential to accelerator plates within the analyzer. Ions are produced using a heated tungsten filament. Thermionically emitted electrons from the filament are accelerated by a 70volt potential to ionize analyte molecules which enter the ionization chamber. Total instrument power consumption will be kept to a 25 watt maximum by using a high efficiency, frequency modulated, filament emission regulator (see APPENDIX A: Emission regulator circuit board layout, pp. 74) and through the use of a permanent magnet to generate the required 3500 Gauss field across the analyzer. The magnet will be constructed in a U-shaped geometry, with an air gap of 1 inch and pole piece diameters of 3.5 inches. Mass will be reduced to approximately 9 kg by fabricating the magnet of NdFeB, with Permendur 49/49/2 alloy pole pieces and yoke (Figure 3.3-2) (also see APPENDIX C: Mechanical drawings, pp. 92-94).

Figure 3.3-2: NdFeB Magnet

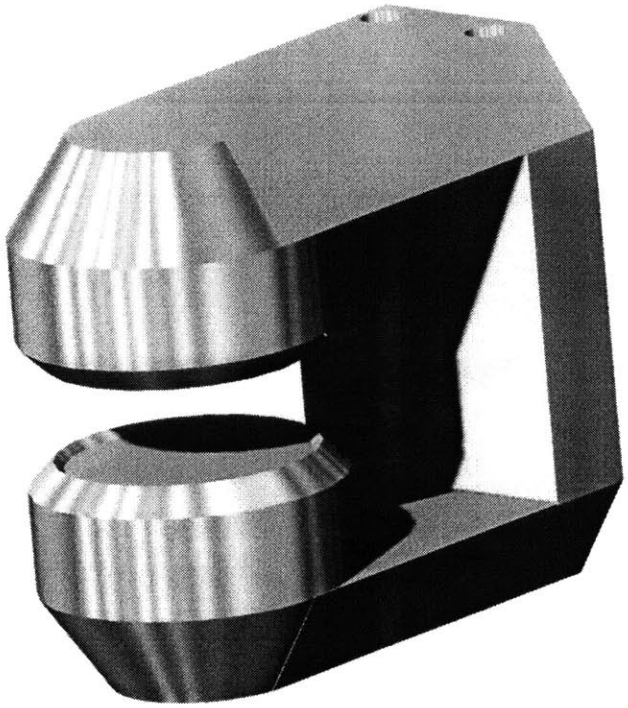

Relative abundance of gases are determined by ion current collection using a Faraday cup. A Faraday cup detector is the only type of sensor possible for the cycloid. Although Faraday cup detectors are less sensitive than other types of sensors (*e.g.* electron multipliers), Faraday cups do possess the inherent advantages of low power consumption and long-term signal stability. Used in conjunction with a low noise electrometer, the detector is capable of sensing ion currents as low as 10^{-14} amps.

3.4 Sensitivity

The inlet system allows for diffusion of analyte gases across the inlet membrane. Given the membrane thickness, surface area, permeability of the membrane to a gas, and the equivalent partial pressure of dissolved gas, a volumetric flux rate of the analyte gas can be estimated. Previous experimentation using a calibrated argon source has indicated that the analyzer requires a minimum gas influx rate of approximately 10^{-12} grams of argon per second (Hemond), or approximately 2.5 $x10^{-14}$ moles of gas per second, to generate a detectable Faraday cup signal. Using this data, minimum MIMS detection limits of individual gas species can be estimated. The minimum mass flux rate of 2.5 $x10^{-14}$ moles/sec can be converted into a minimum volumetric flux rate of 5.6 $x10^{-10}$ cm^3/sec at STP. This flux rate, Q (cm^3 @STP/sec), can then be used to find the equivalent partial pressure, p_1 (atm), of the gas encountered on the external surface of the membrane (Equation 8) (Comyn 1985),

Equation 8:
$$Q\left[\frac{cm^3@STP}{sec}\right] = \frac{P\left[\frac{cm^3@STP \cdot cm}{cm^2 \cdot sec \cdot atm}\right] A[cm^2]}{l[cm]} \left(p_1[atm] - p_2[atm]\right)$$

where permeability coefficient, P ([cm^3@STP·cm]/[cm^2·sec·atm]), of a given gas within the membrane, the membrane surface area, A (cm^2), and membrane thickness, l (cm), are known, and the internal partial pressure of the gas, p_2 (atm), is assumed to be negligible. From this partial pressure, an estimate of minimum detectable dissolved gas concentration can be calculated using Henry's law (see also APPENDIX D: Minimum sensitivity determination, pp. 95-98). Although this model does not account for variables such as variability in ionization efficiency or fragmentation, sensitivity estimates based on the inlet system's physical characteristics correspond reasonably with observed detection limits using this inlet system in conjunction with the Hemond backpack mass spectrometer (Allen 1996) (Figure 3.4-1). These sensitivities will permit MIMS measurement of many common dissolved gases (*e.g.* argon, carbon dioxide, oxygen, and nitrogen) (Seinfeld and Pandis 1998) at ambient concentrations in the ocean, as well as other gases (*e.g.* helium, hydrogen, methane, and hydrogen sulfide) where they occur at elevated concentrations, such as in waters receiving hydrothermal vent fluids, and in anoxic basins (Welhan and Craig 1983; Morel and Hering 1993; Ishibashi, Wakita et al. 1994) (Figure 3.4-2).

Figure 3.4-1: MIMS minimum sensitivities

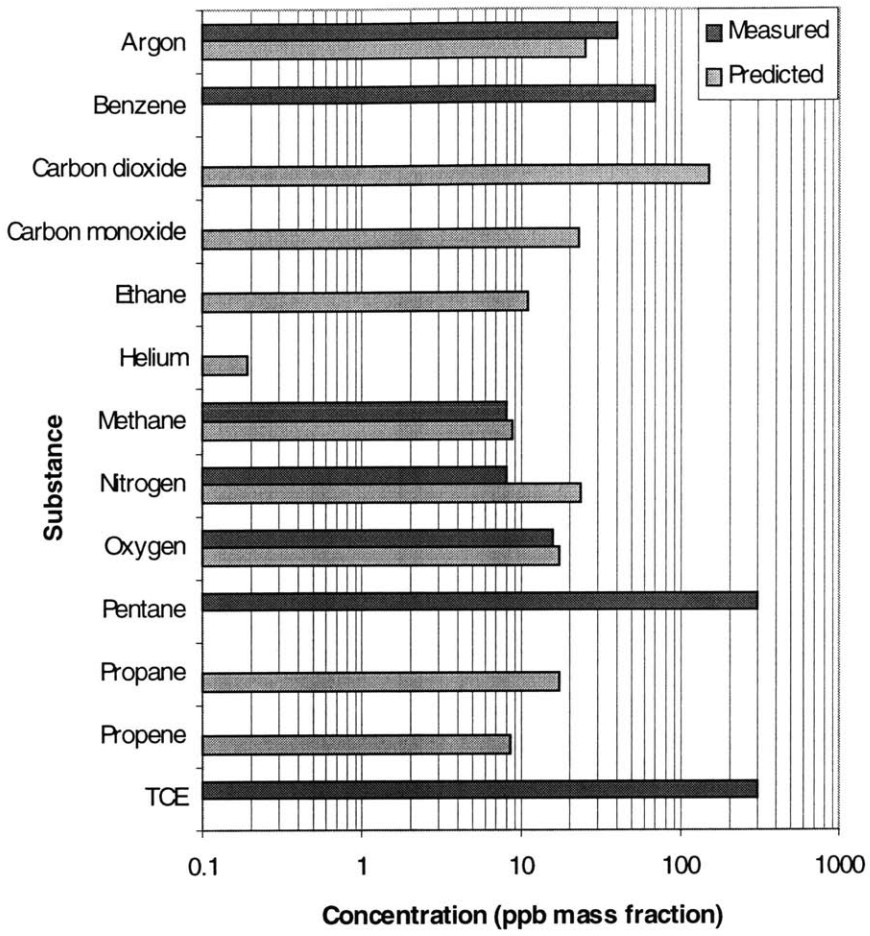

Figure 3.4-2: MIMS minimum sensitivities vs. environmental concentrations

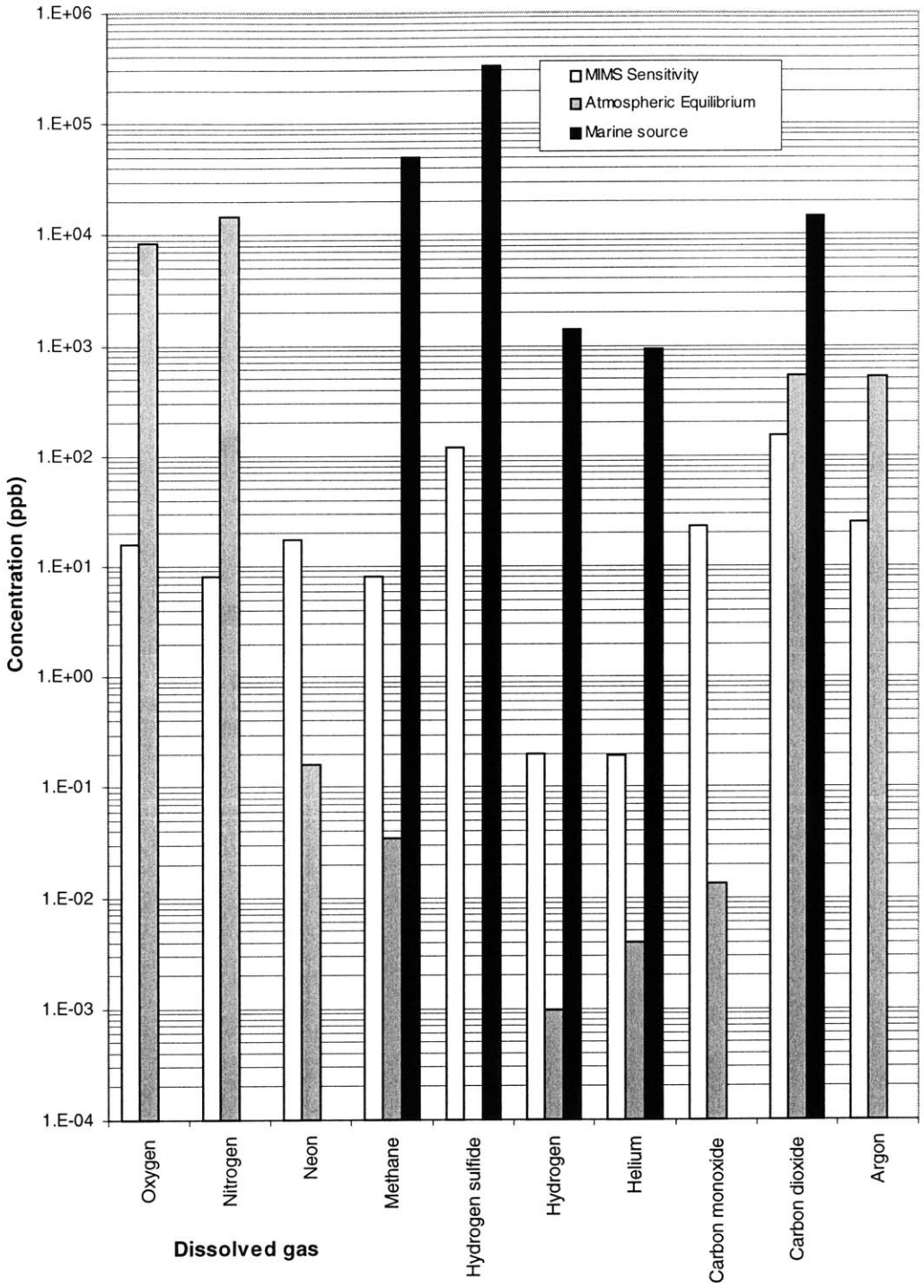

3.4.1 Ionization efficiency

Estimation of instrument sample to signal ratio (approximately equivalent to ionization efficiency) is obtained by comparison of measured minimum electrometer signal threshold against measured minimum analyte influx rates. Given the electrometer input response threshold of 10^{-14}amps, that Faraday cup current is equal to ion current and electrometer input response threshold equals Faraday cup ion current, approximately 60,000 atoms per second are required to generate a minimum detectable signal. By comparison, the observed achievable minimum detection Argon influx rate of 10^{-12} grams per second, indicates that a minimum influx rate of 1.5×10^{10} atoms per second are needed to generate a detectable Faraday cup signal. Therefore, the sample to signal ratio of the instrument, represented as minimum Faraday cup signal divided by minimum influx rate, is approximately 4.1×10^{-6} (ions detected per molecules sampled).

Further improvements in instrument sensitivity may be made through utilization of inlet membranes with improved permeability characteristics, increasing the permeable surface area of the inlet membrane, as well as improving the ionization efficiency of the instrument. Of these possible modifications, improvement in ionization efficiency is presumably of greatest benefit. Increases in permeable surface area have the disadvantage of allowing proportionate increases in water vapor influx. Although utilization of alternative membrane polymers is likely to increase the sensitivity of the instrument to a given gas or group of gases (*e.g.* hydrophobic organics) it is unlikely, given current polymer technology, to identify a polymer with superior permeability characteristics for all gases of interest. In contrast, ionization efficiency increase has no directly associated disadvantages and has the potential for order of magnitude improvements, producing concomitant increases in overall instrument sensitivity.

3.5 Response time

Although a steady-state model is used to estimate sensitivity, several factors result in a non-instantaneous instrument response, including electrometer response time, vacuum system conductance, membrane diffusivity, and diffusivity of gases across the unstirred water boundary layer. The contribution of each delay factor to the instrument's overall response time is unequal. Therefore, the following order-of-magnitude analyses serve to identify the limiting factors for instrument speed.

3.5.1 Membrane

The time required for gases to cross the membrane into the vacuum system can be predicted based on the diffusivity of a given gas within the membrane and on membrane thickness. Provided that the diffusion coefficient of the gas through the polymer is independent of concentration and constant, Fick's second law of diffusion (Equation 9)

Equation 9: $$\frac{\partial C}{\partial t} = -D\left(\frac{\partial^2 C}{\partial X^2}\right)$$

can be applied as a one dimensional diffusive transport model to estimate the rate of gas permeation across the membrane as a function of time, as the system approaches equilibrium (Allen 1989). If the gas concentration on the external surface is kept constant and gas concentration within the vacuum system is effectively maintained at zero, the total gas flux into the vacuum system per permeable surface area, Q_t, can be determined at any point in time (Equation 10).

Equation 10: $$Q_t\left[\text{moles}/\text{cm}^2\right] = \frac{D\left[\text{cm}^2/\text{sec}\right] \cdot C_{ext}\left[\text{moles}/\text{cm}^3\right]}{X\left[cm\right]} \left(t\left[\text{sec}\right] - \frac{X\left[cm\right]^2}{6D\left[\text{cm}^2/\text{sec}\right]} \right)$$

As t approaches ∞, a linear relation between Q_t and t develops, yielding a t-axis intercept, often referred to as time lag, L (sec) (Crank 1975). This time lag can be expressed in terms of membrane thickness, X (cm), and membrane diffusivity, D (cm^2/sec) (Equation 11).

Equation 11: $$L\left[\text{sec}\right] = \frac{X\left[cm\right]^2}{6D\left[\text{cm}^2/\text{sec}\right]}$$

Observation suggests that steady state flow is underestimated by about 4% if a period of approximately three times the time lag is used (Jenkins, Nelson et al. 1970). Applying this time constant of 3L as an estimate of membrane response time, it is evident that membrane thickness strongly affects response time. Given a 1mil membrane thickness, time responses for low molecular weight gases are generally on the order of 10 seconds, with higher molecular weight organics having increased response times (Figure 3.5-1).

Figure 3.5-1: Calculated membrane response time

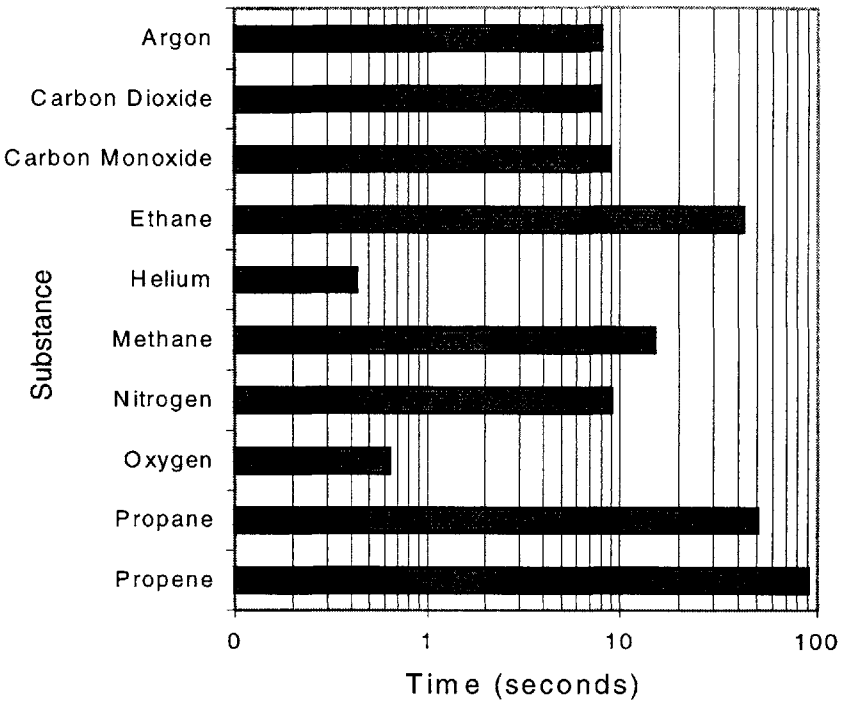

3.5.2 Boundary layer

To the extent that the membrane represents a no-slip boundary condition for water, turbulent transport near the membrane is retarded (Batchelor 1992). Within this stagnant boundary region, transport of gases normal to the membrane surface is principally through molecular diffusion. Stagnant boundary region thickness may be eroded through increased mixing, but is commonly on the order of 10 to 100 μm for water. A maximum water layer response time for the inlet system can be inferred from the diffusion coefficient of the gas of interest in water. Given that the ratio of two gases' molecular diffusion coefficients in water, D, is approximately equal to the inverse of the ratio of the square roots of their molecular weights, MW, (Equation 12:) (Hemond and

Fechner 1994), and using a diffusivity constant of 1.7 x10^{-5} cm^2/sec for carbon dioxide in water, the diffusivity of other molecules in water can be approximated (Figure 3.5-2).

Figure 3.5-2: Mass dependence for molecular diffusion in water

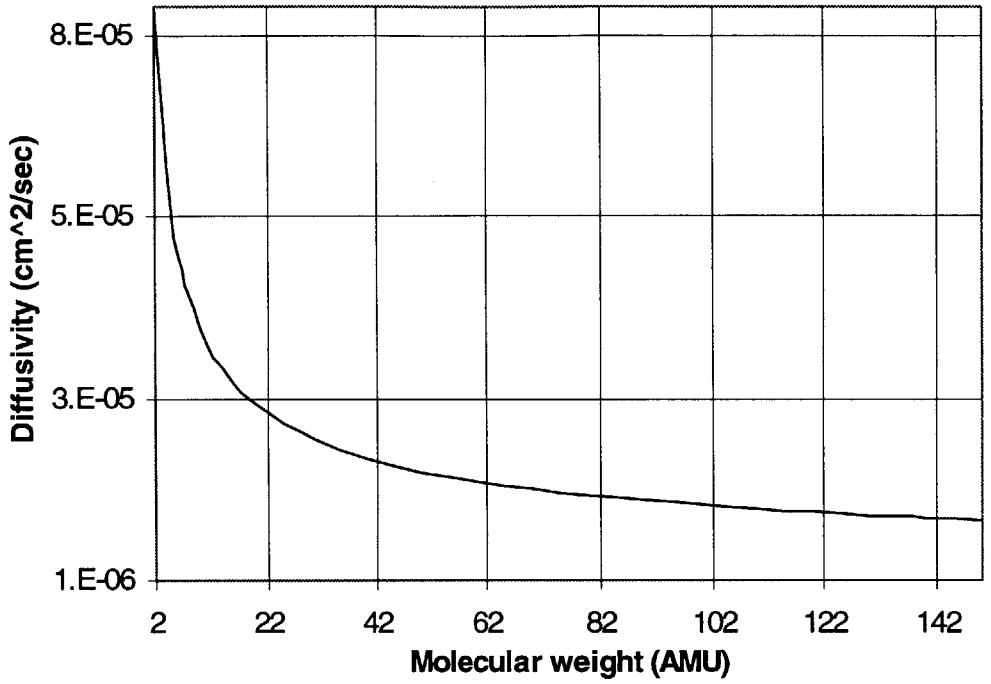

Equation 12: $$\frac{D_A\left[\mathrm{cm}^2/_{\mathrm{sec}}\right]}{D_B\left[\mathrm{cm}^2/_{\mathrm{sec}}\right]} \approx \frac{\sqrt{\mathrm{MW_B}[\mathrm{AMU}]}}{\sqrt{\mathrm{MW_A}[\mathrm{AMU}]}}$$

Assuming that the largest analyte gas of interest will have a mass of 150 AMU (*i.e.* the MIMS mass range limit), a minimum diffusivity can be calculated and applied to the time-to-steady-state lag model. Using a worst case stagnant boundary layer thickness of 100µm, the maximum water time lag for any molecule within the analyzer's mass range is no more than approximately 5 ½ seconds (Figure 3.5-3), and could be decreased by local stirring if necessary.

Figure 3.5-3: Water boundary layer time lag

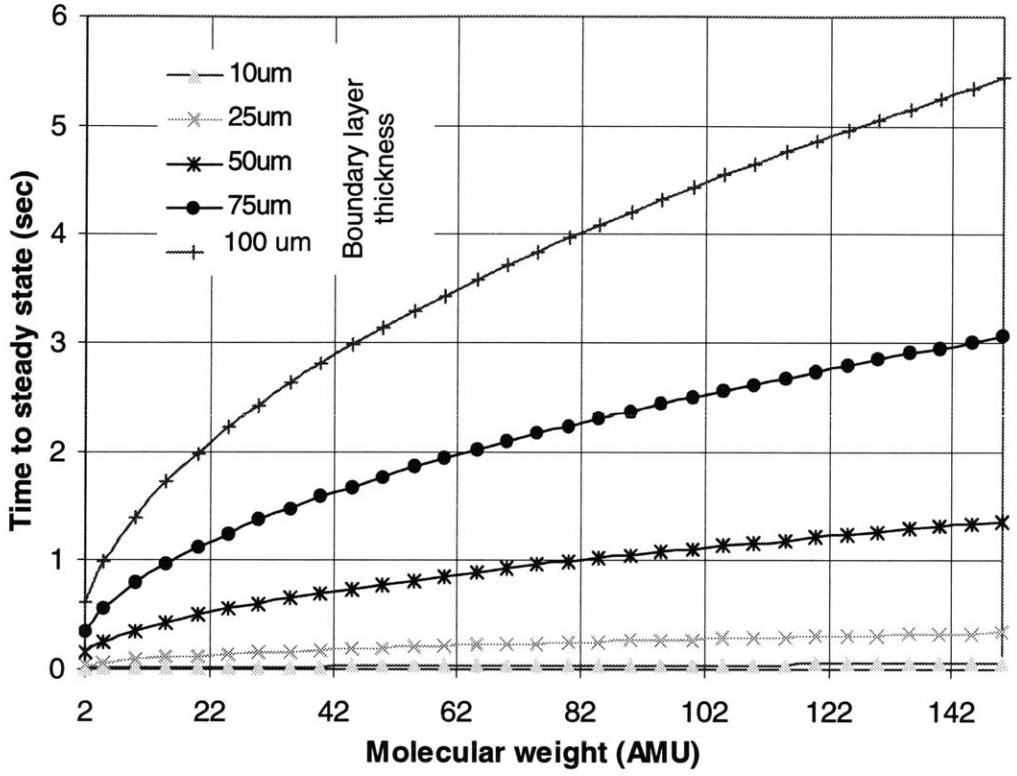

3.5.3 Inlet line

Gas travel from the membrane inlet to the analyzer is an additional source of time delay. This delay is essentially a time offset and can be calculated using a residence time model. Where travel time, t (sec), is simply the volume of the tube, V (cm^3), divided by its conductance, F (cm^3/sec) (Equation 13).

Equation 13: $$t[\text{sec}] = \frac{V[\text{cm}^3]}{F\left[\text{cm}^3/\text{sec}\right]}$$

The operational pressure of the vacuum envelope is approximately 10^{-8} Torr, with the pressure gradient increasing to approximately 10^{-6} Torr along the inlet tube in the direction of the inlet membrane. Therefore, conductance within the inlet tube is modeled

assuming molecular flow conditions (Duschman 1962). In a molecular flow regime, conductance is a function of container geometry, temperature, pressure, and molecular mass; however, it is not dependent on pressure. Using Clausing's approximate solution for conductance (Clausing 1932), a long narrow tube's conductance, F (cm^3/sec), is determined by: tube cross section, A (cm^2); temperature, T (Kelvin); molecular mass, M (AMU); and a dimensionless parameter, K, which is determined by the tube's length to cross sectional area ratio (Equation 14) (see also APPENDIX D: Conductance determinations for vacuum system components, pp. 99).

Equation 14:
$$F\left[{}^{cm^3}/_{sec}\right] = 3638 \times K[_{unitless}] \times A[_{cm^2}] \times \left(\frac{T[_K]}{M[_{AMU}]}\right)^{1/2}$$

Calculations using this model indicate that tube length has the greatest influence on residence time. Based on this analysis, analyte gases of interest have residence times of roughly 1.5 seconds when inlet tube length is 50 cm (Figure 3.5-4).

Figure 3.5-4: Inlet tube residence time

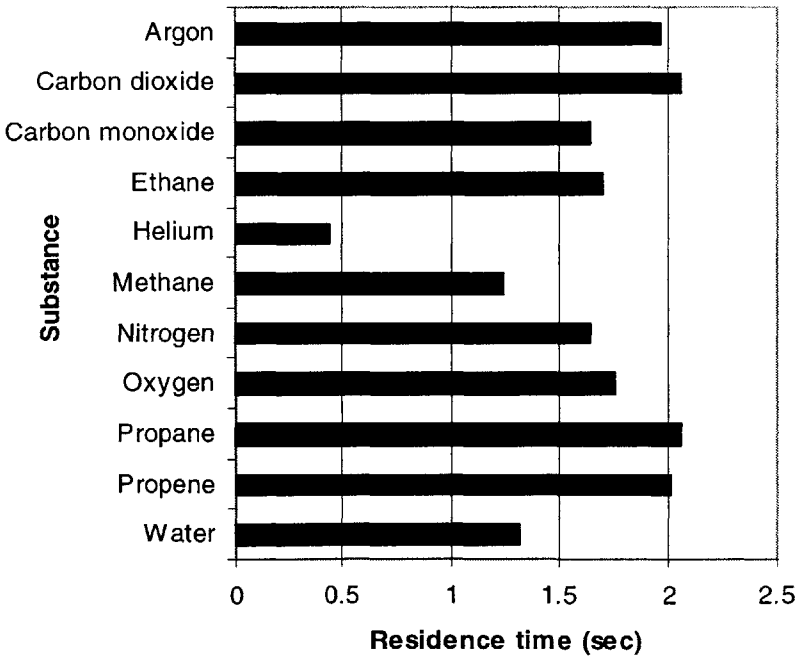

3.5.4 Electrometer

The response time of the electrometer can be described by its RC time constant. The electrometer is based on a Teledyne 1702 op-amp connected as a current-to-voltage converter, followed by a unity gain inverting buffer (Figure 3.5-5). The 1702 has an extremely low bias current achieved with a parametric input stage. A $10^{11}\Omega$ feedback resistor is used in parallel with a 2pF capacitor, giving a response time of approximately one half second.

Figure 3.5-5: Electrometer schematic

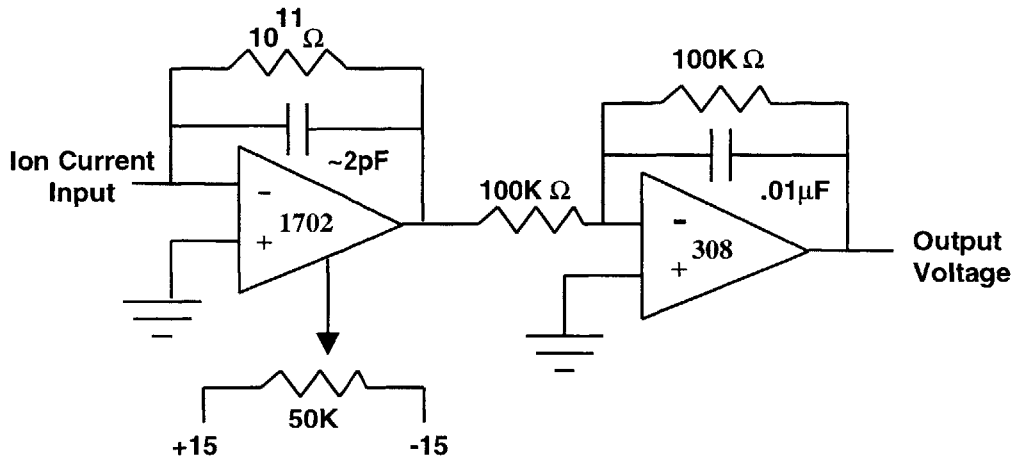

3.5.5 Overall response time

Drawing from the preceding analyses, it is expected that MIMS/AUV response time will be primarily governed by membrane diffusivity if relatively few gas species are being measured, and will be of the order of 10-20 seconds. If successive scans of the entire spectral range are required, electrometer response time may become the limiting factor. For example, if 200 mass peaks (including molecular ions and fragments) are measured per scan, and measurement of each peak requires 0.5 second, the time needed

to complete the scan would be 100 seconds. Further electrometer analysis and re-design may allow for a decreased time constant. Modifications such as use of a smaller input resistor in the first stage would decrease response time and have the added benefit of lowering the resistor's Johnson noise contribution, but would require more detailed analysis of all system noise sources. Development of data interpretation algorithms that predict final electrometer output in advance of the system reaching a steady state value may also help. In a future design, using an electron multiplier instead of a Faraday cup, detector response time could be decreased to milliseconds, under which conditions it would not be a factor.

3.6 Computerized Control

Autonomous operation requires that the MIMS instrument be able to perform all necessary functions via a pre-programmed embedded computer system. Minimum functionality includes powering instrument on & off at predetermined intervals, mass step calibration, accelerator potential control, emission regulator control, data collection & handling, and systems diagnostics. To fulfill these operation needs as well as power and space limitations, the MIMS will use an embedded PC-104 computer coupled with mass selector controller and data acquisition system. The MIMS computer will use a serial port connection to communicate with the AUV control computers.

The controller/data acquisition system, or DAQ board, was designed to function as a compact (12cm x 9 cm), low power (1.5 watt), 16-bit resolution controller and sensor (Figure 3.6-1). It is compatible with computers using 8X86 through Pentium® microprocessors, and interfaces via a printer port employing a PS-2/bi-directional protocol (IEEE1284). The IEEE 1284 standard allows for a maximum data width of 8-

bits. Consequently, the DAQ board makes use of a multiplexor array, which allows for a "two pass" 16-bit transfer of both controller and sensor data. The DAQ board relies on an Analog Devices 569 digital-to-analog converter to "write" commands to the mass selector and an Analog Devices 7884 analog-to-digital converter to "read" electrometer voltage. Both the 7884 and the 569 possess sample-and-hold capabilities, permitting simultaneous operation of the DAQ's input and output.

Figure 3.6-1: DAQ board

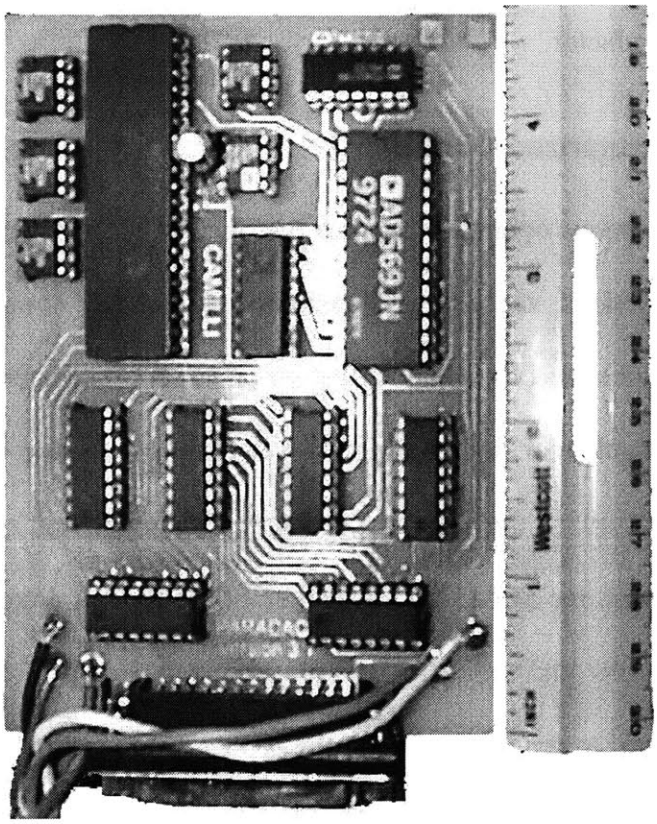

3.6.1 Power

During the development and testing of the DAQ board, an Hewlett Packard 6236B controlled voltage source was used to supply the +5V and -5V required and an Heath 2718 to supply +12V and -12V. The DAQ board consumes approximately 1.5

watts of power, requiring a +5V supply sourcing 20 mA, a -5V supply sinking 20 mA, a +12V supply sourcing 40 mA, a -12V supply sinking 40 mA, and GND.

3.6.2 Board fabrication & layout

The DAQ board was fabricated from a dual sided copper photo-etched board. Photo-resist etching mask negatives were drawn using TurboCAD version 2.0 software. The footprint of the DAQ board measures 4.8 x 3.5 inches and is designed to be compatible with PC-104 form factor. The DAQ board is in its third generation of design and is denoted as PARADAQ version 3.1 on the board surface (see Appendix A: PARADAQ and emission regulator circuitry). Previous design generations employed a prototype Analog Devices AD7882 analog-to-digital converter which has since been abandoned by Analog Devices, because of bugs within the converter. The board is designed to allow for sockets to be soldered into place, permitting replacement of individual integrated circuits. All socket pads are designed for DIP integrated circuits. Future versions of the DAQ board can be made smaller by replacing the AD7884 with an AD7885, which eliminates the need for two of the six multiplexors, and by using surface-mount integrated circuits.

3.6.3 Software

DAQ BOARD software was written using the Q-Basic language. Q-Basic was chosen because code for the backpack-portable mass spectrometer, which uses an RS232 serial port, was written in Quick Basic 4.0 (Microsoft's predecessor to Q-Basic). The code for the backpack mass spec was modified slightly to accommodate the new parallel port interface. All software written for the parallel port interface requires a computer operating on a MS-DOS platform and possessing a Bi-directional (PS2) parallel port

operating within the HEX address range of &H378-&H37A and using a BYTE mode handshaking protocol (Figure 3.6-2). The DAQ software is not written to support SPP (also known as nibble mode), EPP, ECP, nor FIFO mode handshaking protocols.

Figure 3.6-2: DAQ board timing diagram

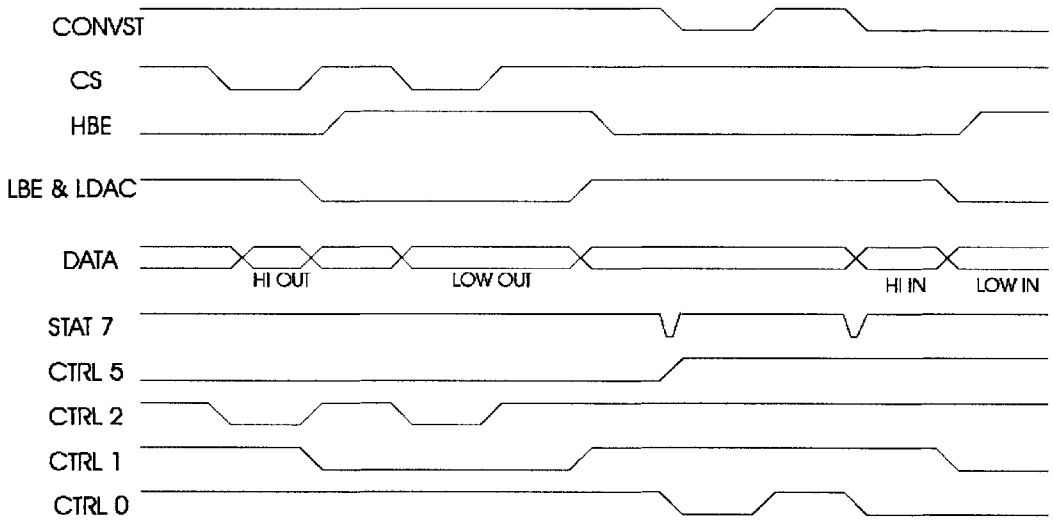

All Q-Basic programs written for the DAQ board use direct memory addressing, or DMA, to read and write information to and from a parallel port residing in the computer's LPT1 range. This LPT1 address corresponds to a hexadecimal address of 378h. From this address, the three parallel port registers can be accessed: the data register at 378h, the status register at 379h, and the control register at 37Ah. Operation of the DAQ board is accomplished via a standard execution code for IEEE-1284 standard bi-directional parallel port equipped computers (see APPENDIX B: Standard PARADAQ execution code pp. 81). A modified execution code has been developed for computers such as the Toshiba T1000 notebook computer, which uses a variation on the IEEE-1284

standard (control bit 7 replacing the functioning of control bit 5)[2] (see APPENDIX B: Toshiba T1000 PARADAQ execution code, pp. 85). Analog-to-digital converter command values for the Toshiba T1000 should have a value of 96 added (adding bit 7, and subtracting bit 5).

The output portion of the code first writes the output values to the AD569 in a "two pass" method, then the input commands switch the control register lines to read the data register AD7884 input values, in a "two pass" method as well (Figure 3.6-3).

Figure 3.6-3: DAQ board controller subroutine

```
MSB = INT(BITCNT / 256)
LSB = INT(BITCNT - MSB * 256)
REM OUTPUT TO DA CONVERTER FIRST HIGH, THEN LOW
OUT &H37A, 4
OUT &H378, MSB
OUT &H37A, 0
OUT &H37A, 4
OUT &H37A, 6
OUT &H378, LSB
OUT &H37A, 2
OUT &H37A, 6
OUT &H37A, 4

REM INPUT READ FROM AD CONVERTER
OUT &H37A, 165
OUT &H37A, 164
OUT &H37A, 165
hibyte = INP(&H378)
OUT &H37A, 167
lobyte = INP(&H378)
inbits = (hibyte * 256) + (lobyte)
```

[2] The IEEE 1284 standard specifies that control register lines 0,1, and 3 use inverted logic.

3.6.4 Speed

Speed measurements were conducted using five different host computers (a Winbook XL Pentium 233MHz, a Dell Dimension 486DX 66MHz, a Dell Dimension Pentium 60Mhz, a Dolch 386 16MHz with math coprocessor, and a Toshiba T1000 8088 9.8MHz). Using each computer, the DAQ board was made to execute a testing code which cycled through successive read and write commands across the voltage input and output range (Figure 3.6-4) (see APPENDIX B: High-speed PARADAQ testing code, pp. 78). Speed of execution was then measured using a Tektronics 2230 digital oscilloscope connected to the output of the DAQ board (AD569 output) and was determined by time period of individual voltage steps for the controller and by distance between AD7884 BUSY signal pulses. To better approximate the speed liability of a Windows based DAQ, time values were measured with and without MS Windows loaded. Results indicate that execution speed is slowed by at least a factor of two when MS Windows is loaded, with an even greater slowing observed when other programs are open.

Figure 3.6-4: DAQ operation speed

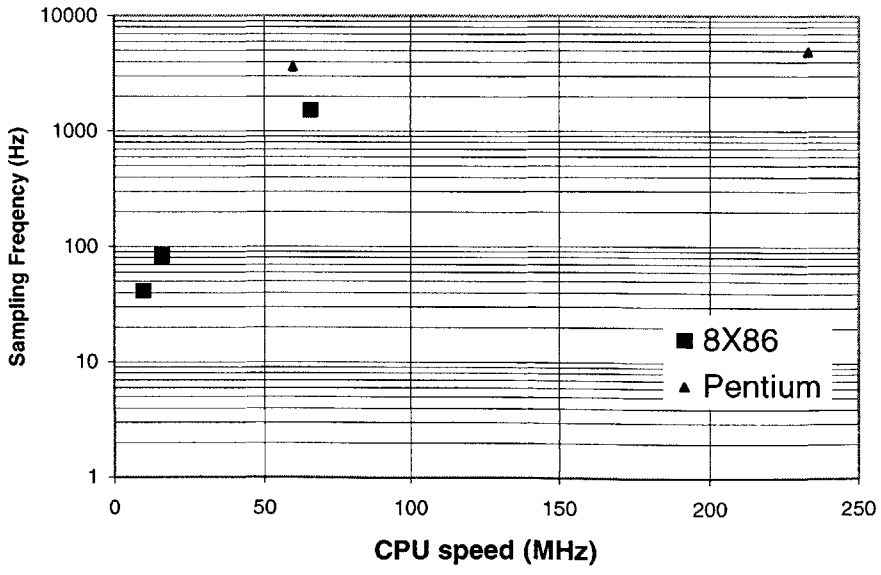

Although sampling frequency appears to plateau as CPU speed approaches 75MHz, accuracy does not diminish with increased execution speed, suggesting that the absolute execution rate limit of the DAQ Board may be in excess of the measured 233MHz system performance; conceivably approaching the 100 kHz range[3]. Although untested, there are other factors aside from CPU speed which may limit the DAQ board sampling frequency, including the Parallel Port UART speed, bus speed, and the software/code efficiency. If increased sampling frequency is desired for future operation, a low-cost solution could be to re-write the execution code in a compileable language such as C or C++; thus avoiding the time penalty of an interpreter and thereby increasing the DAQ board speed.

Based on the data (Figure 3.6-4), the greatest hardware-derived performance increase occurs between the 386 and 486 systems. Although higher frequency Pentium® based systems offer the highest performance, it comes at a cost and energy use premium (Figure 3.6-5). Given the power constraints of approximately 5 watts for the AUV-mass spectrometer computer and DAQ board, a 486 based PC-104 system running at 66Mhz represents the upper limit of available performance at this time. Therefore, a sampling rate upper limit of approximately 1.5 kHz can be expected for the AUV mass spectrometer system if the Qbasic command code is used.

Although 1.5 kHz is several orders of magnitude faster than the response time of the existing electrometer (the present rate-limiting factor), the excess capability can be used for purposes of signal averaging; thus permitting increased accuracy. Other, slower, types of analog-to-digital converters (*i.e.* integrating digital-to-analog converters) may be as accurate as the AD7884, given the present electrometer response time, but would be

[3] AD7884 conversion rate limit is 166 kSPS

incompatible with a faster electrometer. Therefore, the AD7884's speed is advantageous in that the DAQ circuitry does not need to be altered to accommodate future electrometer designs with faster response times.

Figure 3.6-5: PC-104 clock speed vs. power consumption[4]

System	CPU speed	Watts
386	25	2.5
486	66	4
Pentium	133	7.5

3.6.5 Accuracy

Error correction algorithms have been incorporated into the DAQ board execution code to increase accuracy. The output (digital-to-analog conversion) correction is simply a computed 4mV offset (digital equivalent of 26.2 DEC), while the input (analog-to-digital conversion) correction is a slope-offset algorithm designed to accommodate a 2's complement architecture. To further decrease sampling error, a signal-averaging subroutine has been developed for the analog-to-digital conversion subroutine. This signal averaging routine takes 100 samples, which are averaged together and then assigned to one data point. Using these error correction strategies, the DAQ board has demonstrated input and output capabilities with 16-bit accuracy (Figure 3.6-6).

[4] from Ampro PC-104 data sheets

Figure 3.6-6: DAQ error (using correction algorithm & signal averaging)

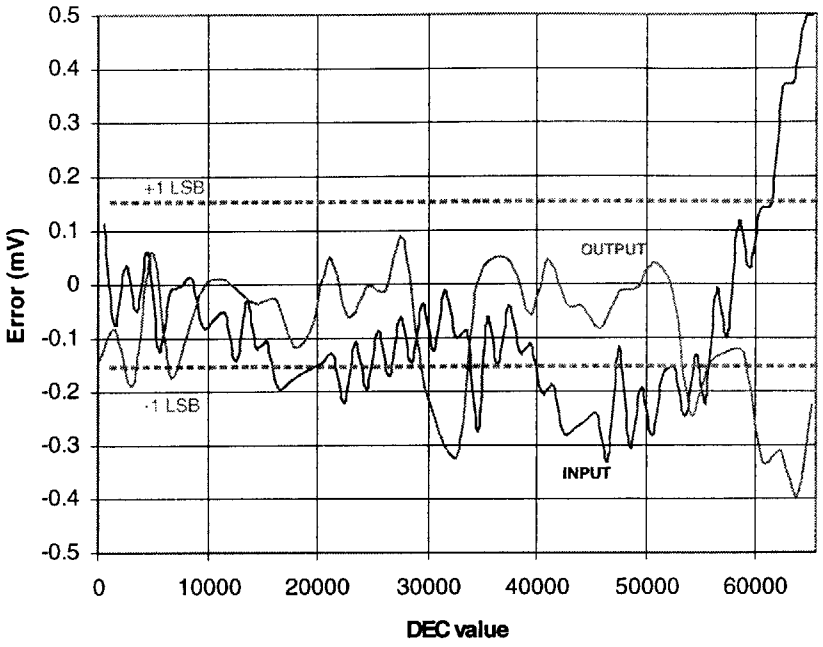

To assess its DAQ output (digital-to-analog), input (analog-to-digital), and an overall high-speed (input reading output) accuracy, three different types of accuracy measurements were conducted on the DAQ board. All three DAQ system accuracy test programs were executed on a Dell Dimension 60 desktop computer.

Output measurements were conducted using the DAQ board to generate a voltage at the output of the DAQ digital-to-analog converter (see APPENDIX B: PARADAQ digital-to-analog conversion testing code pp. 75). This voltage value was then measured using a Keithley 199 System DMM/Scanner. Based on values written to the AD569 digital-to-analog converter versus DMM voltage readings (Figure 3.6-7), the DAQ output has a nearly undetectable deviation from linearity ($R^2 \approx 1$), and an average offset error of -380 μVolts. This error fell largely in the deficit range, with actual voltage generated being less than expected. Therefore, the controller routine was modified to include an

equivalent 2-bit offset[5], thus bringing the DAQ output performance to within an average error tolerance of less than 1 least significant bit (1 LSB).

Figure 3.6-7: DAQ output error (using error correction algorithm)

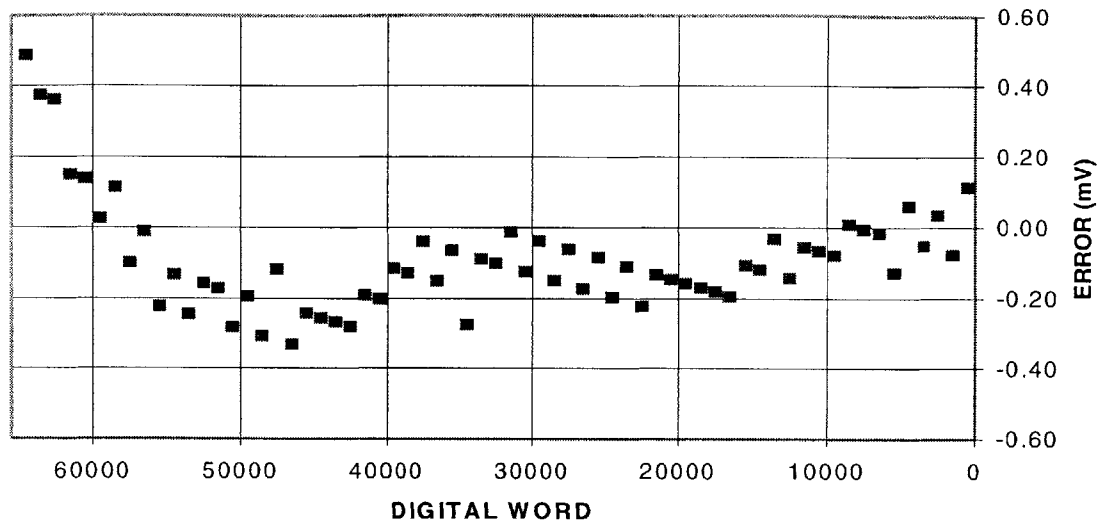

To measure input accuracy, an Hewlett Packard 6236B voltage source, paired with a tunable voltage divider, was used to generate DC potentials (+5v to -5v range) which were recorded with the DAQ's AD7884 analog-to-digital converter, (see APPENDIX B: PARADAQ analog-to-digital conversion testing code pp. 77). These values were then compared with Keithley DMM values. DAQ input test data (each data point constructed from 100 signal averaged samples) exhibited an average accuracy of approximately 99.935% (average error 6.54 mV) across the entire 10 volt scale (Figure 3.6-8). By examining the input error "fingerprint" (error patterns appear to be unique to each AD7884), a reproducible pattern of error was found. It was then possible to write an error correction algorithm into the DAQ input testing code. With the incorporation of this error correction algorithm (in addition to 100x sampling), the average accuracy was

[5] 1LSB ≈ 153μV

increased to approximately 99.999%, or an average error of ±105μV (Figure 3.6-9). Thus, the DAQ input demonstrated an operational error rate of less than 1 LSB.

Figure 3.6-8: DAQ input error (using 100x signal averaging without error correction algorithm)

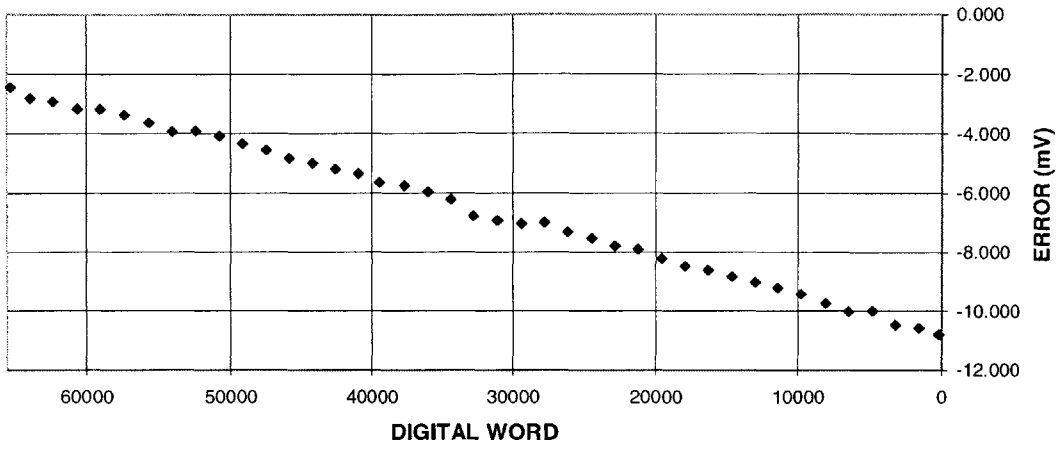

Figure 3.6-9: DAQ input error (using 100x signal averaging with error correction algorithm)

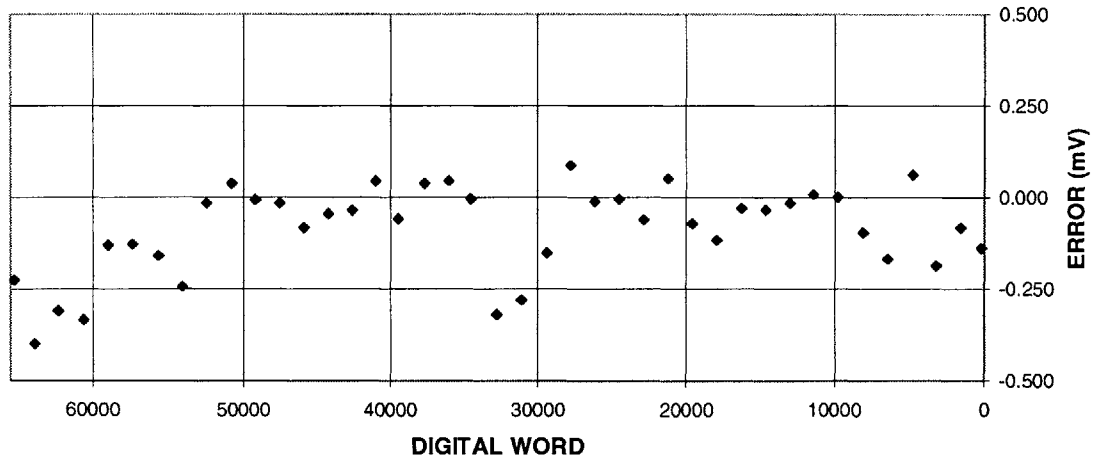

For the overall high-speed accuracy test, each bit in the entire 16-bit digital range was measured. To conduct this test the DAQ system executed a testing code in which the AD569 digital-to-analog output generated a voltage that was then read back directly to the AD7884 analog-to-digital input (see APPENDIX B: High-speed PARADAQ testing code pp. 78). Test data revealed a 93.9μV average error across the entire range of 65,536 control steps. Based on the 6,553,600 data samples taken (each data point composed of 100 data samples), the majority of error occurred in the +5V region of the spectrum (Figure 3.6-10). A possible explanation for this error trend is that a gain or offset error originating in the AD588 voltage reference causes a reference error in the +5V region of the conversion. The AD588 supports only a 12bit absolute accuracy; higher accuracy requires additional trimming potentiometers to correct offset and gain errors. This error pattern resurfaces as a slightly more exaggerated trend in the output test data (Figure 3.6-7). The DAQ input error may therefore be canceling out portions of the DAQ output error in the high-speed testing procedure.

Figure 3.6-10: Overall high speed DAQ error

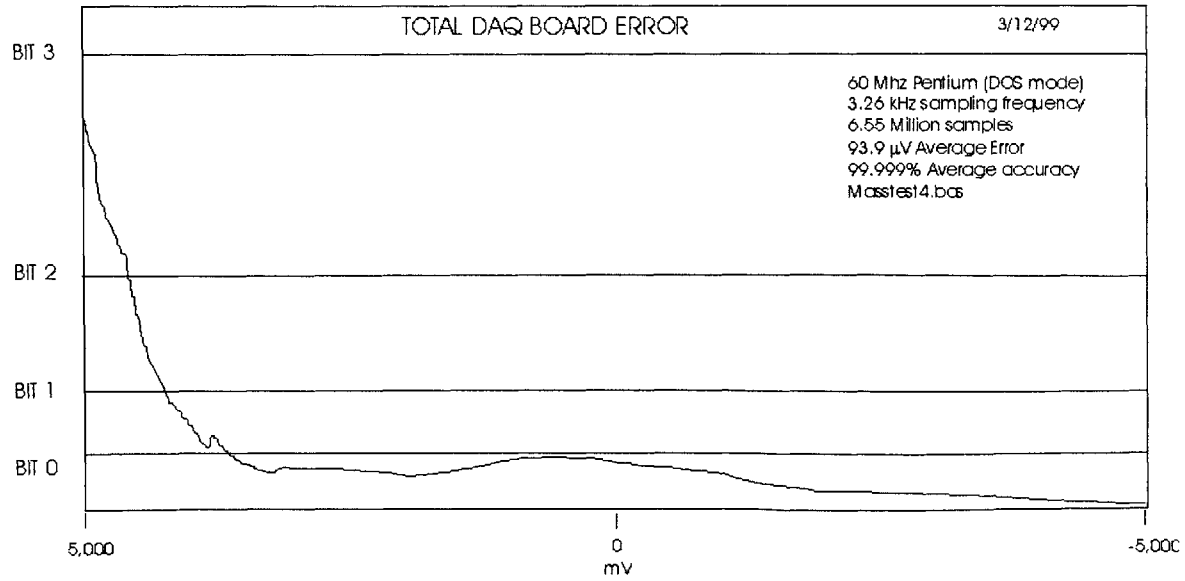

3.7 Data handling

Considering the discrete nature of data point generation and the continuous diffusion of gases across the membrane inlet, data values can be considered a temporal average of the gas concentrations encountered between successive measurements. If the MIMS is operating while moving spatially (*e.g.* onboard an Odyssey AUV), data points can be described as a one-dimensional temporal and spatial average of gas concentrations encountered during the sampling interval.

With a sampling rate of 1 data point per second, and each data point having a 16-bit value, the MIMS would generate 7.2 kilobytes of data per hour of operation. Additional memory overhead would be required to label data points with time values; therefore, assuming each data point is augmented with a 2 byte time and mass value signature, the memory requirement expands to 14.4 kilobytes per hour of operation. Most modern data storage media are thus capable of storing several weeks worth of raw MIMS data. One conceivable solution for MIMS data storage is to use a flashable solid-state (PC card) disk. These devices have the advantages of extremely small form factor, low power consumption, high tolerance to vibration, impact, and pressure fluctuation, low cost, and ease of transfer from the MIMS computer to a laptop (*i.e.* physically exchangeable cards). For example, a 64Mb solid-state disk (commonly used in digital cameras) would be able to store approximately 180 days worth of unprocessed MIMS data. A storage system of this type allows for raw data to be periodically downloaded to a land-based computer for processing using spectrum separation software based on the UNMIX algorithm (Doherty 1987).

3.8 Packaging

The AUV/MIMS prototype will be designed to fit within a 17-inch glass Benthos pressure sphere, which is the standard payload container for an Odyssey class AUV. The upper hemisphere of the pressure sphere will house the analyzer and ancillary components including embedded computer, DAQ board, electrometer, emission regulator board, ion pump, magnet, and power supply (Figure 3.8-1). These items will be held in place using a framework mounted to a standard support ring in the lower hemisphere. Volume within the lower hemisphere has been reserved for a Yardney Silvercel LR12-3 battery to power the instrument, which will permit at least 12 hours of continuous MIMS operation without recharge. The membrane inlet will be positioned outside the pressure sphere, on the hull of the AUV. Connection from the inlet system to the analyzer will be accomplished with a small diameter (approximately 2mm) flexible stainless steel inlet tube, traversing the lower hemisphere through a standard penetration point.

Figure 3.8-1: MIMS layout

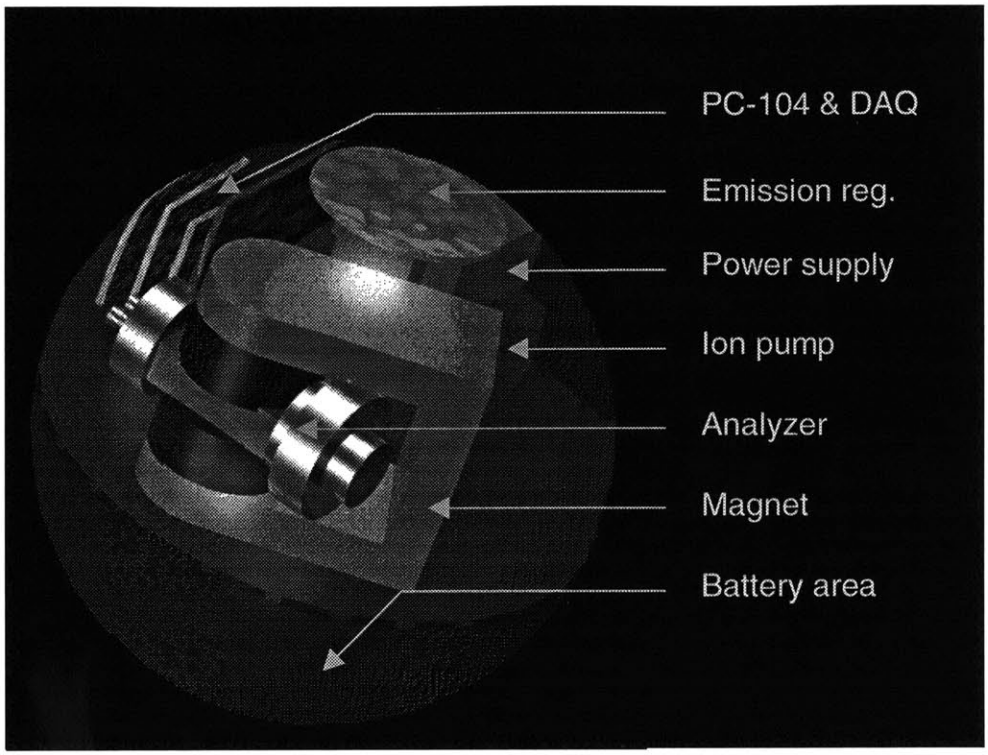

3.9 Calibration

Once the instrument is assembled, self-calibration procedures must be implemented for the MIMS to accurately take data. To assist the MIMS in self-calibration, a dissolved oxygen sensor and a temperature sensor will also be incorporated into the MIMS package. These sensors will be used by the MIMS computer to provide calibration references during MIMS operation. The dissolved oxygen sensor will be used as a periodic reference for sensor drift compensation, and the temperature sensor will provide continuous temperature data to account for changes in membrane permeability caused by temperature variation. Along with the oxygen and temperature sensors, diagnostic and mass selector self-calibration subroutines must be developed for the imbedded computer. Mass selector calibration can be accomplished by using a small

mass step (< 0.01 AMU) scan to find the centers of three reference peaks of commonly found gases/gas molecule fragments (*e.g.* N_2, OH, O_2) and then assigning accelerator potential values to computed mass values. After these scan algorithms have been completed, calibrations for sensitivity and peak height will be conducted using individual dissolved gas standards of known concentration, cross referenced by GC-MS analysis of the standards. Finally, data storage and transfer subroutines will be developed for the embedded computer.

REFERENCES

1. Allen, G. (1989). Comprehensive Polymer Science. New York, Pergamon.
2. Allen, G. (1996). Final Report: Mass Spectrometers. Cambridge, Massachusetts Institute of Technology: unpublished.
3. Alper, J. (1990). "Oases in the oceanic desert." ASM American Society for Microbiology News **56**(10): 536-538.
4. Axelson, J. (1996). Parallel Port Complete. Madison, WI, Lakeview Research.
5. Batchelor, G. (1992). An Introduction to Fluid Dynamics. Cambridge, UK, Cambridge University Press.
6. Bates, T. S., K. C. Kelly, et al. (1996). "A Reevaluation of the Open Ocean Source of Methane to the Atmosphere." Journal of Geophysical Research **101**(D3): 6953-6961.
7. Baykut, G. and J. Franzen (1994). "Mobile Mass Spectrometry; a decade of field applications." Trends in Analytical Chemistry **13**(7): 267-274.
8. Bellingham, J. G. (1997). Hunting Giant Squids with AUVs - An Informal Summary. Cambridge, MIT Sea Grant College Program.
9. Bellingham, J. G., C. A. Goudey, et al. (1992). A small, long-range autonomous vehicle for deep ocean exploration. Proceedings of the Second International Offshore and Polar Engineering Conference, San Francisco.
10. Bellingham, J. G., B. A. Moran, et al. (1996). Haro Strait Experiment 1996. Cambridge, MIT Sea Grant College Program.
11. Bleakney, W. and J. Hipple (1938). "A New Mass Spectrometer with Improved Focusing Properties." Physical Review **53**: 521-527.
12. Bussmann, I. and E. Suess (1998). "Groundwater seepage in Eckernfoerde Bay (Western Baltic Sea): Effect on methane and salinity distribution of the water column." Continental Shelf Research [Cont. Shelf Res.] **18**(14-15): p. 1795-1806.
13. Clausing, P. (1932). Ann. Physik **12**: 961.
14. Comyn, J. (1985). Polymer permeability. New York, Elsevier Applied Science.
15. Conrad, R. and W. Seiler (1988). "Methane and Hydrogen in Seawater (Atlantic Ocean)." Deep-Sea Research **35**(12): 1903-1917.
16. Conrad, R. and W. Seiler (1988). "Methane and hydrogen in seawater (Atlantic Ocean)." Deep-Sea Res. (a Oceanogr. Res. Pap.) **35**(12): p. 1903-1917.
17. Crank, J. (1975). The Mathematics of Diffusion. New York, Oxford University Press.
18. Dafner, E., A. Obzhirov, et al. (1998). "Distribution of methane in waters of the Okhotsk and western Bering Seas, and the area of the Kuril Islands." Hydrobiologia **362**(1-3): p. 93-101.
19. Doherty, R. (1987). An Algorithm for Mixture Component Determination for use in Membrane Inlet Mass Spectrometry. Civil Engineering. Cambridge, Massachusetts Institute of Technology: 272.
20. Duschman, S. (1962). Scientific Foundations of Vacuum Technique. New York, Wiley.
21. Ernst, M. (1994). Modeling Multicomponent Vacuum Flow, Transport, and Outgassing in a Membrane-Inlet Vapor Sampling Probe. Civil and Environmental Engineering. Cambridge, Massachusetts Institute of Technology: 345.
22. Fingas, M. and C. Brown (1997). "Remote sensing of oil spills." Sea Technology [Sea Technol.] **38**(9): p. 37-46.

23. Hemond, H. laboratory data. Cambridge, Massachusetts Institute of Technology: unpublished.
24. Hemond, H. and E. Fechner (1994). Chemical Fate and Transport in the Environment. San Diego, Academic Press.
25. Hemond, H. F. (1991). "A Backpack-portable Mass Spectrometer for Measurement of Volatile Compounds in the Environment." Rev. Sci. Instrum. **62**: 1420.
26. Ishibashi, J. I., H. Wakita, et al. (1994). "Helium and carbon geochemistry of hydrothermal fluids from the North Fiji Basin spreading ridge (southwest Pacific)." Earth and Planetary Science Letters [EARTH PLANET. SCI. LETT.] **128**(3-4): p. 183-197.
27. Jenkins, R., P. Nelson, et al., Eds. (1970). . Transactions of the Faraday Society.
28. Johnson, J. (1999). "Evaluation of a Seawater Equilibrator for Shipboard Analysis of Dissolved Oceanic Trace Gases." Analytica Chimica Acta **395**: 119-132.
29. Kiser, R. (1965). Introduction to Mass Spectrometry and Its Applications. Toronto, Prentice Hall.
30. Lehr, W., J. Galt, et al. (1996). Tracking the North Cape Oil Spill. Proceedings of the 19th Arctic and Marine Oilspill Program Technical Seminar.
31. Martens, C. S. (1976). Methane production, consumption, and transport in the interstitial waters of coastal marine sediments. Benthic Processes and the Geochemistry of Interstitial Waters of Marine Deposits, Edinburgh, UK, THE DYNAMIC ENVIRONMENT OF THE OCEAN FLOOR.
32. Morel, F. M. and J. G. Hering (1993). Principles and Applications of Aquatic Chemistry. New York, Wiley-Interscience.
33. Park, S. (1995). "Surface Seawater Sampling Device During Navigation." Ocean Research **17**(1): 59-63.
34. Pauly, S. (1999). Polymer Handbook. New York, Wiley-Interscience Publication.
35. Reddy, C. M. and J. G. Quinn (1999). "GC-MS Analysis of Total Petroleum Hydrocarbons and Polycyclic Aromatic Hydrocarbons in Seawater Samples After the North Cape Oil Spill." Marine Pollution Bulletin [Mar. Pollut. Bull.] **38**(2): p. 126-135.
36. Richardson, L. (1988). A Field-Usable Membrane-Probe Mass Spectrometer. Civil Engineering. Cambridge, Massachusetts Institute of Technology: 62.
37. Roark, R. and W. Young (1975). Formulas for Stress and Strain. New York, McGraw-Hill.
38. Sander, R. (1999). Compilation of Henry's Law Constants for Inorganic and Organic Species of Potential Importance in Environmental Chemistry. Mainz, Germany, Max-Plank Institute of Chemistry: 98.
39. Sansone, F. J., T. M. Rust, et al. (1998). "Methane distribution and cycling in Tomales Bay, California." Estuaries **21**(1): p. 66-77.
40. Scranton, M. I. and K. McShane (1991). "Methane fluxes in the southern North Sea: The role of European rivers." Continental Shelf Research **11**(1): 37-52.
41. Seinfeld, J. and S. N. Pandis (1998). Atmospheric Chemistry and Physics From Air Pollution to Climate Change. New York, Wiley-Interscience.
42. Takahashi, T., C. Wunsch, et al. (1993). Applications of Analytical Chemistry to Ocean Carbon Cycle Studies. Washington, D.C., National Research Council: Committee on Oceanic Carbon, Ocean Studies Board, Commission on Geosciences, Environment, and Resources: 85.

43. Tilbrook, B. D. and D. M. Karl (1995). "Methane sources, distributions and sinks from California coastal waters to the oligotrophic North Pacific gyre." Marine Chemistry [MAR. CHEM.] **49**(1): p. 51-64.
44. Tsurushima, N., S. Watanabe, et al. (1996). "Methane in the East China Sea water." Journal of Oceanography. Tokyo [J. OCEANOGR.] **52**(2): p. 221-233.
45. Wakeham, S. G. (1992). Sampling and Experimental Challenges for the Next Decade in Marine Organic Chemistry - a Prospectus. DOC/DON Workshop, Honolulu, HI.
46. Welhan, J. A. and H. Craig (1983). Methane, hydrogen and helium in hydrothermal fluids at 21 degree N on the East Pacific Rise. NATO Advanced Research Institute Conference: Hydrothermal Processes At Seafloor Spreading Centers., Cambridge, UK.

Appendix A: PARADAQ and emission regulator circuitry

PARADAQ integrated circuit descriptions

An Analog Devices 7884 analog-to-digital converter is used to "read" electrometer voltage. The AD7884 is a 16-bit monolithic analog-to-digital converter with internal sample-and-hold and a conversion time of 5.3 μs. It uses a two pass flash architecture and has a maximum throughput rate of 166 kSPS. Two input ranges are available: ±5 V and ±3 V. Conversion is initiated by the CONVST signal, and the result is read using the CS and RD inputs. The AD7884 has a 16-bit parallel reading structure and conversion results are expressed in 2s complement.

An Analog Devices 569 digital-to-analog converter to "write" commands to the mass selector. The AD569 is a monolithic 16-bit digital-to-analog converter (DAC), which can operate in either unipolar or bipolar modes; nominal reference range is ±5V. Data may be loaded into the AD569's input latches from 8- and 16-bit buses; four TTL/LSTTL/5 V CMOS-compatible signals control the latches: CS, LBE, HBE, and LDAC.

An Analog Devices 780 voltage reference is used to provide a stable +3 V reference for the AD7884 analog to digital converter. The AD780 is a precision bandgap reference voltage which provides a 2.5 V or 3.0 V output from inputs between 4.0 V and 36 V.

Four Analog Devices 817 operational amplifiers function as buffers and an inverter for the AD7884 analog-to-digital converter. These low power, single/dual supply, high speed op-amps have a 50 MHz unity gain bandwidth, 350 V/μs slew rate and settling time of 45 ns. Previous generations of DAQ boards, designed without high

speed op-amp buffers, were plagued by parasitic oscillations which severely limited converter resolution.

An Analog Devices 588 voltage reference is utilized to provide a stable +5v reference for the AD569 digital-to-analog converter. The AD588 is a monolithic voltage reference which uses an ion-implanted buried Zener diode and laser trimmed internal resistors. It is capable of 12 bit absolute accuracy and the following outputs: ±5 V, +5 V and +10 V, –5 V & –10 V dual outputs or +5 V, –5 V, +10 V, –10 V single outputs.

A Harris CD4011 quad 2 input CMOS NAND gate functions as a logic inverter for the digital-to-analog converter high byte/low byte write enable. As of this writing, Harris semiconductor has been sold to Intersil and this NAND gate is available in a CD4011BT version.

A total of six Motorola MC14551B multiplexors are used as data bus switches, allowing for the reading or writing of 8 bits of data in parallel. The MC14551B is a quad 2 input digitally controlled analog multiplexor, with a break before make switch function. This line of Motorola semiconductors is now sold under the manufacturer name ON Semiconductor.

PARADAQ schematic

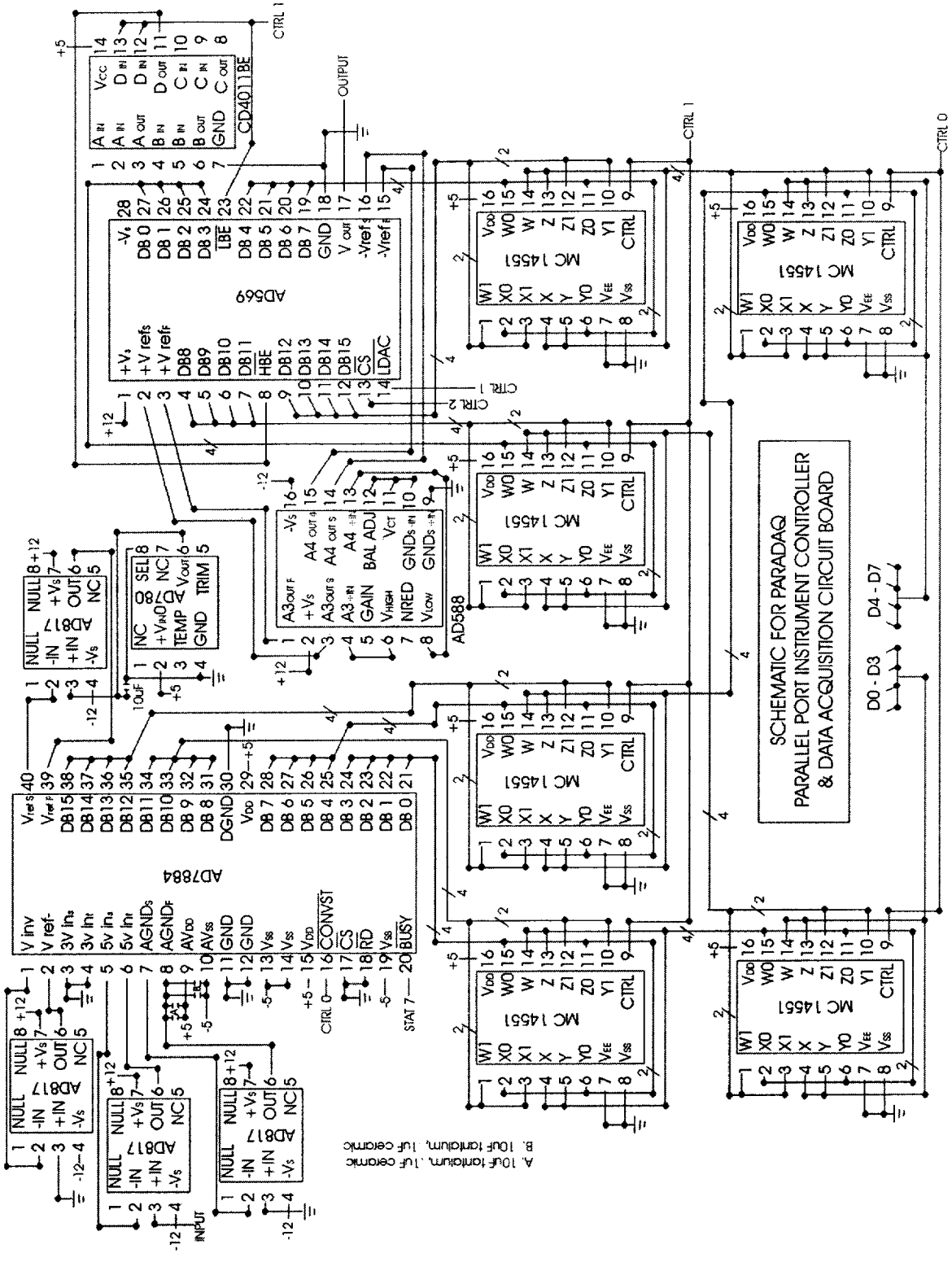

PARADAQ circuit board modifications

There are a total of 10 modifications required when building the DAQ from a PARADAQ version 3.1 etched board. They are as follows:

1. No ground trace for the (7884 linked, byte select row, inner position) Motorola 14551 MUX. To correct this, jumper the orphaned ground to the neighboring ground on the outer MUX.
2. CTRL0 (pin 1 of the parallel port socket) trace goes to !CS (pin 17 of the 7884) on the 7884; it should go to the !CONVST (pin 16 of the 7884). To correct this, cut the trace and jumper properly. Then, jumper the !CS (pin 17 of the 7884) to trigger from CTRL2 (pin 16 of parallel port socket).
3. The !LBE (pin 23 of the 569) needs to be jumpered to the CTRL1 (pin 14 of the parallel port socket) trace.
4. The $\pm 3V_{IN}S$ and $\pm 3V_{IN}F$ pins of the AD7884 (pins 3 and 4 respectively) need to be tied to $AGND_F$ (pin 8 of the AD7884).
5. AD7884 data bits 9 and 10 are reversed (pins 32 and 33 respectively). To correct this, cut traces and switch connections with jumpers.
6. Two decoupling capacitors (10µF tantalum and 0.1µF ceramic in parallel) must be added to AV_{DD} (pin 9 of the AD7884) and AV_{SS} (pin 10 of the AD7884), directly at the pins, which connect each to AGND (pin 8 of the AD7884).
7. One decoupling capacitor (1µF ceramic) between V_{DD} (pin 15 of the AD7884) and GND (pin 11 of the AD7884), as well as between V_{SS} (pin 13 of the AD7884) and GND (pin 12 of the AD7884) must be added.
8. !RD (pin 18) and !CS (pin 17) of the AD7884 must be jumpered together.
9. !CS (pin 13 of the AD569) must be jumpered to CTRL2 (pin 16 of parallel port socket).
10. !LDAC (pin 14 of the AD569) must be jumpered to the CTRL1 (pin 14 of the parallel port socket) trace.

PARADAQ circuit layout (etched version 3.1)

Upper stack plane

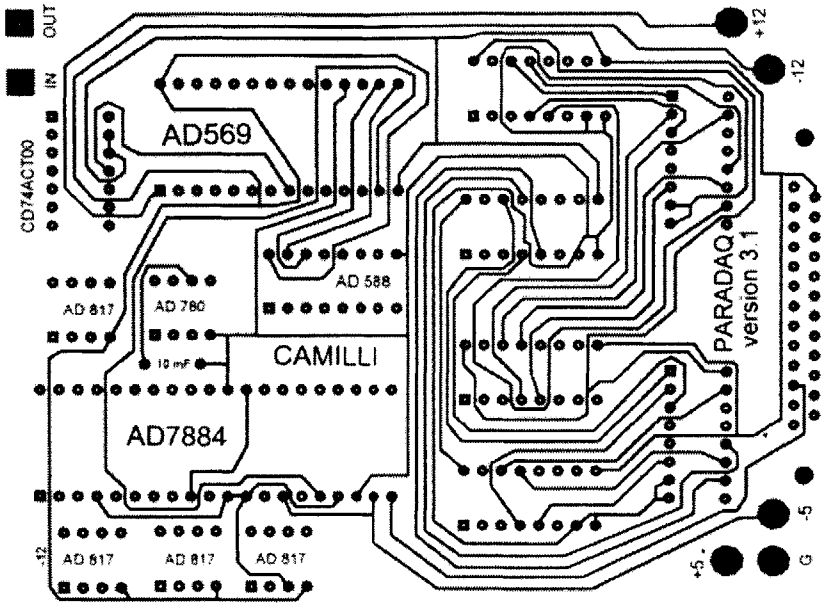

Lower stack plane

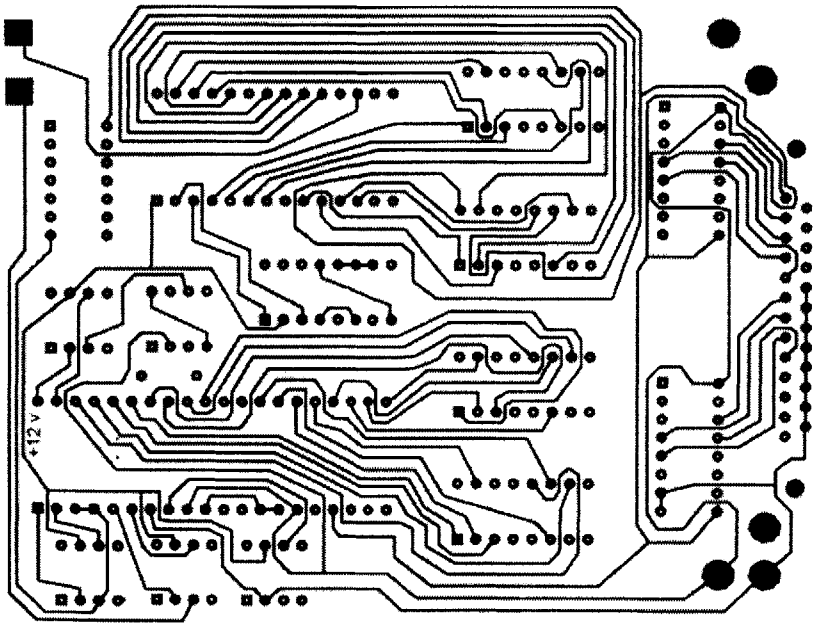

Register Bit assignments for PARADAQ parallel port connector

PARADAQ name	Assignment
Data bit 0	input/output data bit 0
Data bit 1	input/output data bit 1
Data bit 2	input/output data bit 2
Data bit 3	input/output data bit 3
Data bit 4	input/output data bit 4
Data bit 5	input/output data bit 5
Data bit 6	input/output data bit 6
Data bit 7	input/output data bit 7
Busy	read 7884 busy signal
CTRL 0	7884/569 data select
CTRL 1	high/low byte select
CTRL 2	569 chip select
CTRL 3	unused
CTRL 5	standard input/output select
CTRL 7	Toshiba T-1000 input/output select

Pin assignments for D-sub (IEEE 1284-A) parallel port connector[6]

PARADAQ name	Register bit	Signal pin	Ground return pin
Data bit 0	D0	2	19
Data bit 1	D1	3	19
Data bit 2	D2	4	20
Data bit 3	D3	5	20
Data bit 4	D4	6	21
Data bit 5	D5	7	21
Data bit 6	D6	8	22
Data bit 7	D7	9	22
Unused	S3	12	24
Unused	S4	13	24
Unused	S5	15	23
Unused	S6	10	24
Busy	S7!	11	23
CTRL0	C0!	1	18
CTRL1	C1!	14	25
CTRL2	C2	16	25
CTRL3	C3!	13	24

[6] from (Axelson 1996)

Emission regulator circuit board layout

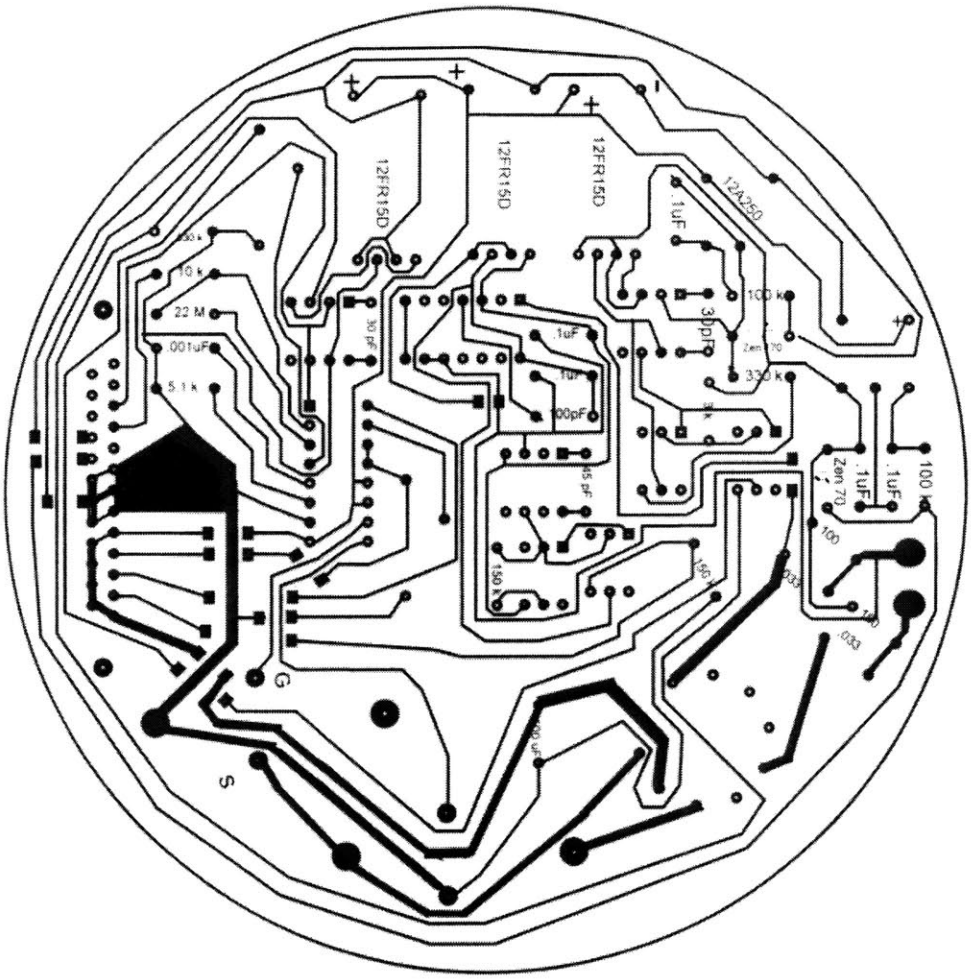

APPENDIX B: Computer code

PARADAQ digital-to-analog conversion testing code

```
800 REM SCANNING ROUTINE
    indarr = 1
    count = 1

810 REM START OF SCAN LOOP
860 davolts = 65536 - indarr
865 IF davolts < 0 THEN PRINT "END OF ROUTINE"
866IF davolts < 0 THEN GOTO 960
870 BITCNT = davolts
880 msb = INT(BITCNT / 256)
890 lsb = INT(BITCNT - msb * 256)

891 REM OUTPUT TO DA CONVERTER FIRST HIGH, THEN LOW
900 OUT &H37A, 4
901 OUT &H378, msb
902 OUT &H37A, 0
903 OUT &H37A, 4
904 OUT &H37A, 6
905 OUT &H378, lsb
906 OUT &H37A, 2
907 OUT &H37A, 6
908 OUT &H37A, 4

910 indarr = indarr + 1000
    count = count + 1

950 REM SCREEN DISPLAY
    REM VGA IS X = 640 PIXELS, Y = 480 PIXELS (EACH LINE/COLUMN IS 8)
    CLS
    SCREEN 11
    PRINT "   DAQ board Controller Testing Options"
    PRINT "   Select option, then press ENTER"
    PRINT "  "
    PRINT "     1) OUTPUT NEXT DATA STEP"
    PRINT "     2) EXIT"
    LOCATE 15, 20
    PRINT "Digital Word=", BITCNT
    LOCATE 16, 20
    PRINT "         mV=", ((BITCNT - 32767) / 6.5535)
    LOCATE 16, 50
    PRINT "           "
    INPUT "OPTION CHOICE?", IX
    IF IX = 1 THEN GOTO 810
    IF IX = 2 THEN END
```

```
960 REM SCREEN DISPLAY
    REM VGA IS X = 640 PIXELS, Y = 480 PIXELS (EACH LINE/COLUMN IS 8)
    CLS
    SCREEN 11
    PRINT "   DAQ board Controller Testing Options"
    PRINT "   Select option, then press ENTER"
    PRINT "  "
    PRINT "     1) RESTART"
    PRINT "     2) EXIT"
    INPUT "OPTION CHOICE?", IX
    IF IX = 1 THEN GOTO 800
    IF IX = 2 THEN END
```

PARADAQ analog-to-digital conversion testing code

```
100  REM PARADAQ sensor testing code
     REM INPUT READ FROM AD CONVERTER
     count = 0
     TOTVOLTS = 0
     TOTBITS = 0

200  IF count > 99 THEN GOTO 600
     count = count + 1
     OUT &H37A, 37              'starts conversion
     OUT &H37A, 36              'reads hibyte
     OUT &H37A, 37
     HIBYTE = INP(&H378)
     OUT &H37A, 39              'reads lowbyte
     LOWBYTE = INP(&H378)
     IF HIBYTE > 127 THEN GOTO 400 ELSE GOTO 300

300 INBITS = (HIBYTE * 256) + LOWBYTE
     GOTO 500

400 INBITS = ((HIBYTE * 256) + LOWBYTE) - 65536

500 TOTBITS = TOTBITS + INBITS
     GOTO 200

600 REM VGA IS X = 640 PIXELS, Y = 480 PIXELS (EACH LINE/COLUMN IS 8)
     CLS
     SCREEN 11
     PRINT "  DAQ board Sensor Testing Options"
     PRINT "  Select option, then press ENTER"
     PRINT "  "
     PRINT "    1) TAKE DATA"
     PRINT "    2) EXIT"
     LOCATE 14, 20
     PRINT "Digital Word AVG.=", TOTBITS / count
     LOCATE 15, 20
     RAWVOLTS = (TOTBITS / (count * 32.768) * 5)
     PRINT "w/o correction mV  =", RAWVOLTS
     LOCATE 16, 20
     REM the + 2.2 onward is for error correction
     CORRECTEDVOLTS = (TOTBITS / (count * 32.768) * 5) + 2.2 - ((((TOTBITS /
(count * 32.768) * 5) - 5000) / 10000) * 8.5)
     PRINT "w/  correction mV =", CORRECTEDVOLTS
     INPUT "OPTION CHOICE?", IX
     IF IX = 1 THEN GOTO 100
     IF IX = 2 THEN END
```

High-speed PARADAQ testing code

```
100 REM VGA IS X = 640 PIXELS, Y = 480 PIXELS (EACH LINE/COLUMN IS 8)
200 CLS
210 SCREEN 11
220 LINE (32, 8)-(632, 350), , B
250 LOCATE 6, 6
260 PRINT "---------------------------------- BIT 4 ----------------------------------"
    LOCATE 1, 2
    PRINT "mV"
    LOCATE 6, 1
    PRINT "1.2"
270 LOCATE 14, 6
280 PRINT "---------------------------------- BIT 3 ----------------------------------"
    LOCATE 14, 1
    PRINT "0.6"
290 LOCATE 18, 6
300 PRINT "---------------------------------- BIT 2 ----------------------------------"
    LOCATE 18, 1
    PRINT "0.3"
    LOCATE 20, 6
    PRINT "----------------------------------- LSB -----------------------------------"
    LOCATE 20, 1
    PRINT ".15"

310 LOCATE 22, 3
320 PRINT "0"
330 LOCATE 23, 5
340 PRINT "65536                    <-OUTPUT->"
350 LOCATE 23, 79
360 PRINT "0"
370
380 REM END OF SUBOUTINE*********************************************************
400 REM SCANNING ROUTINE
    indarr = 1
    cnt = 1
430 REM START OF SCAN LOOP
460 davolts = 65536 - indarr
465 IF davolts < 0 THEN GOTO 1500
470 BITCNT = davolts
480 msb = INT(BITCNT / 256)
490 lsb = INT(BITCNT - msb * 256)
491 REM OUTPUT TO DA CONVERTER FIRST HIGH, THEN LOW
500 OUT &H37A, 4
501 OUT &H378, msb
502 OUT &H37A, 0
503 OUT &H37A, 4
504 OUT &H37A, 6
505 OUT &H378, lsb
506 OUT &H37A, 2
507 OUT &H37A, 6
```

```
508 OUT &H37A, 4
510 indarr = indarr + 1
    cnt = cnt + 1
520 REM DELAY LOOP************************************************************


610 REM INPUT READ FROM AD CONVERTER
    count = 0
    TOTVOLTS = 0
    TOTBITS = 0
    RAWVOLTS = 0
    CORRECTEDVOLTS = 0

620 IF count > 99 THEN GOTO 700
    count = count + 1
    OUT &H37A, 37              'starts conversion
    OUT &H37A, 36              'reads hibyte
    OUT &H37A, 37
    HIBYTE = INP(&H378)
    OUT &H37A, 39              'reads lowbyte
    LOWBYTE = INP(&H378)
    IF HIBYTE > 127 THEN GOTO 685 ELSE GOTO 680

680 INBITS = (HIBYTE * 256) + LOWBYTE
   GOTO 690

685 INBITS = ((HIBYTE * 256) + LOWBYTE) - 65536

690 TOTBITS = TOTBITS + INBITS
   GOTO 620

700 outvolts = ((((msb * 256) + lsb) / 6.5535)) - 4999.6
    RAWVOLTS = (TOTBITS / (count * 32.768) * 5)
    REM the + 2.2 onward is for error correction
    CORRECTEDVOLTS = (TOTBITS / (count * 32.768) * 5) + 2.2 - ((((TOTBITS /
(count * 32.768) * 5) - 5000) / 10000) * 8.5)

751 rawsum = (outvolts - RAWVOLTS)
    IF rawsum < 0 THEN rawsum = rawsum * (-1) ELSE GOTO 752

752 IF rawsum < .3 THEN rawsum = 0 ELSE rawsum = rawsum
    tot = tot + rawsum
    av = (tot / cnt)

754 correctsum = (outvolts - CORRECTEDVOLTS)
    IF correctsum < 0 THEN correctsum = correctsum * (-1) ELSE GOTO 755



755 IF correctsum < .3 THEN correctsum = 0 ELSE correctsum = correctsum
    totCOR = totCOR + correctsum
```

```
    avCORR = (totCOR / cnt)
    LOCATE 1, 20
    PRINT "     7000X MAGNIFICATION OF FULL SCALE      "
    LOCATE 4, 20
    PRINT "ERROR W/O CORRECTION (Mv)", av
    LOCATE 3, 50
    PRINT "      "
    LOCATE 3, 20
    PRINT "ERROR W/CORRECTION (Mv)  ", avCORR
    PRINT "     "
    LOCATE 25, 40
    PRINT "Digital Word=", (TOTBITS / count)
    PRINT "         "
    LOCATE 26, 40
    PRINT "                                  "
    LOCATE 27, 40
    PRINT "                                  "
    LOCATE 25, 1
    PRINT "                                "
    LOCATE 26, 40
    PRINT "    Sense mV=", CORRECTEDVOLTS
    PRINT "         "
    LOCATE 27, 40
    PRINT "  Control mV=", outvolts
    PRINT "         "
    LOCATE 25, 1
    PRINT "Samp Err mV=", outvolts - CORRECTEDVOLTS
    PRINT "         "
1055 GOTO 1079
1077 REM THIS IS IN VOLTS...EXPECT -5V TO 5V
1078 REM PLOT DATA
1079 GOSUB 1120
1080 MASS = MASS + MSTEP
1081 GOTO 460
1090 RETURN
1100 REM END OF SCAN ROUTINE**************************************************
1110 REM
1120 REM PLOT SCAN ON SCREEN - MASS VS LOG (INVOLTS * 1000)
1130 XVAL = 32 + 600 * (65536 - davolts) / (65536)
1152 YVAL = 349 - (avCORR * 228)
1153 GOTO 1170
1170 IF MASS = MMIN THEN LINE (XVAL, YVAL)-(XVAL, YVAL) ELSE GOTO 1190
1180 RETURN
1190 LINE -(XVAL, YVAL)
1200 RETURN
1210 REM END OF SUBROUTINE****************************************************
1250 END
1500 END
```

Standard PARADAQ execution code

(For use with the Hemond backpack mass spectrometer)

```
1  GOSUB 280
   DIM ARRAY(200)
2  CLS
   PRINT "Mass Spectrometer Control Options"
   PRINT "Select option, then press ENTER"
   PRINT " "
   PRINT "1) DISPLAY SPECTRUM FROM DISK"
   PRINT "2) SCAN"
   PRINT "3) CALIBRATE"
   PRINT "4) EXIT"
   INPUT "OPTION CHOICE?", IX
   IF IX = 1 THEN GOSUB 1250
   IF IX = 2 THEN GOSUB 10
   IF IX = 3 THEN GOSUB 400
   IF IX = 4 THEN END
   GOTO 2
10 REM SCAN OPTION
40 REM DISPLAY/GET PARAMETERS
50 GOSUB 150
60 REM SETUP SCREEN
70 GOSUB 580
105 GOSUB 800
110 RETURN
130 REM END OF MAIN PROGRAM**************************************************
140 REM
150 REM DISPLAY PARAMETERS
160 PRINT "Minimum M/Z", MMIN
170 PRINT "Maximum M/Z", MMAX
180 PRINT "M/Z Step", MSTEP
190 PRINT "Settling Time", STLTIM
200 PRINT "Read Time", RTIME
210 PRINT "Calibrate Slope", CALSLOPE
220 PRINT "Offset", OFFSET
221 IF PLOTTYP$ = "LG" THEN PRINT "Logarithmic Plot"
222 IF PLOTTYP$ = "LN" THEN PRINT "Linear Scale; Scalefactor =", SCLEFACT
230 INPUT "NEW PARAMETERS? (Press N for new parameters, ENTER for scan)",
    YN$

240 IF YN$ = "n" THEN GOSUB 400 ELSE RETURN
250 GOTO 150
260 REM END OF SUBROUTINE****************************************************
270 REM
280 REM INITIALIZE SUBROUTINE
290 MMIN = 12
300 MMAX = 150
310 MSTEP = .5
320 STLTIM = 1
```

```
330 RTIME = 1
340 CALSLOPE = 53.36
350 OFFSET = 0
351 PLOTTYP$ = "LN"
352 SCLEFACT = 14.5
360 RETURN
370 REM END OF SUBROUTINE**************************************************
380 REM
390 STOP
400 REM PARAMETERS SUBROUTINE
410 INPUT "Minimum M/Z", X
420 IF X > .1 THEN MMIN = X
430 INPUT "Maximum M/Z", X
440 IF X > .1 THEN MMAX = X
450 INPUT "M/Z Step", X
460 IF X > .1 THEN MSTEP = X
470 INPUT "Settling Time", X
480 IF X > .1 THEN STLTIM = X
490 INPUT "Read Time", X
500 IF X > .1 THEN RTIME = X
510 INPUT "Calibration Slope", X
520 IF X > .1 THEN CALSLOPE = X
530 INPUT "Offset", X
REM 540 IF X > .1 THEN OFFSET = X
541 INPUT "Linear (LN) or Logarithmic (LG) Plot Desired?", X$
542 IF X$ = "LN" THEN PLOTTYP$ = "LN" ELSE PLOTTYP$ = "LG"
543 INPUT "Scale Factor for Linear Plot", X
544 IF X > .1 THEN SCLEFACT = X
550 RETURN
560 REM END OF SUBROUTINE**************************************************
570 REM
580 REM SETUP SCREEN
590 REM VGA IS X = 640 PIXELS, Y = 480 PIXELS (EACH LINE/COLUMN IS 8)

600 CLS
610 SCREEN 11
620 LINE (32, 8)-(632, 155), , B
630 LOCATE 2, 2
640 PRINT "10"
650 LOCATE 6, 3
660 PRINT "8"
670 LOCATE 10, 3
680 PRINT "6"
690 LOCATE 14, 3
700 PRINT "4"
710 LOCATE 18, 3
720 PRINT "2"
730 LOCATE 21, 3
740 PRINT MMIN
750 LOCATE 21, 76
760 PRINT MMAX
```

```
770 RETURN
780 REM END OF SUBOUTINE*********************************************************
790 REM
800 REM SCANNING ROUTINE
810 ERASE ARRAY
820 INDARR = 0
830 REM START OF SCAN LOOP UNTIL MASS >MMAX
850 MASS = MMIN

REM 860 DAVOLTS = CALSLOPE / MASS + OFFSET
REM 870 BITCNT = 6553.5 * DAVOLTS

860 DAVOLTS = 862502.2762188# / (MASS + OFFSET)
870 BITCNT = DAVOLTS - 5746.1838018659#
880 MSB = INT(BITCNT / 256)
890 LSB = INT(BITCNT - MSB * 256)
891 REM OUTPUT TO DA CONVERTER FIRST HIGH, THEN LOW
900 OUT &H37A, 4
901 OUT &H378, MSB
902 OUT &H37A, 0
903 OUT &H37A, 4
904 OUT &H37A, 6
905 OUT &H378, LSB
906 OUT &H37A, 2
907 OUT &H37A, 6
908 OUT &H37A, 4
910 INDARR = INDARR + 1
920 REM DELAY LOOP***********************************************************
930 FOR I = 1 TO STLTIM
940 NEXT I
REM 970 FOR I = 1 TO 5
REM 980 NEXT I
990 GOTO 1020
REM IF LOC(1) > 0 THEN GOTO 1020 ELSE LOCATE 10, 10
991 REM DON'T THINK 990 & 1000 WILL WORK
1000 PRINT "NO RESPONSE FROM INTERFACE"
1010 RETURN
1019 REM INPUT READ FROM AD CONVERTER
1020 OUT &H37A, 37
1021 OUT &H37A, 36
1022 OUT &H37A, 37
1023 hibyte = INP(&H378)
1024 OUT &H37A, 39
1026 lobyte = INP(&H378)
1040 inbits = (hibyte * 256) + (lobyte)
1045 inbytes = INT(inbits)
       IF inbytes > 32767 THEN GOTO 1046 ELSE GOTO 1050
1046 inbolts = (((inbytes - 65536) / 32768) * 5) + 5
      GOTO 1051
1050 inbolts = ((inbytes / 32768) * 5) + 5
1051 involts = inbolts + .002 + ((inbolts / 65536) * .008)
```

```
        LOCATE 21, 40
        PRINT "Digital Word=", inbytes
        LOCATE 22, 40
        PRINT "         mV=", involts * 1000
        LOCATE 21, 15
        PRINT "LOWBYTE =", lobyte
        LOCATE 22, 15
        PRINT "HIGHBYTE=", hibyte
1055 GOTO 1079
1077 REM THIS IS IN VOLTS...EXPECT -5V TO 5V
1078 REM PLOT DATA
1079 GOSUB 1120
1080 MASS = MASS + MSTEP
1081 IF MASS > MMAX THEN GOTO 1082 ELSE GOTO 860
1082 CLOSE
1083 LOCATE 24, 5
1084 INPUT "Type 1 to abandon spectrum file, ENTER to Save ", IY
        IF IY = 1 THEN RETURN
        INPUT "Please type the filename of spectrum file", NAME$
        OPEN NAME$ FOR OUTPUT AS #2
        FOR IZ = 1 TO INDARR
        WRITE #2, ARRAY(IZ)
        NEXT IZ
        REM THE FILE CONTAINS A SPECTRUM WITH EVEN ELEMENTS=MASS
        REM THE FOLLOWING EVEN ELEMENTS=VOLTAGE
1090 RETURN
1100 REM END OF SCAN ROUTINE**************************************************
1110 REM
1120 REM PLOT SCAN ON SCREEN - MASS VS LOG (INVOLTS * 1000)
1130 XVAL = 32 + 600 * (MASS - MMIN) / (MMAX - MMIN)
1150 IF involts < .001 THEN involts = .001
1151 IF PLOTTYP$ = LG$ THEN GOTO 1160
1152 YVAL = 154 - (involts * SCLEFACT)
1153 GOTO 1170
1160 YVAL = 154 - (LOG(1000 * involts)) * 15.2
1170 IF MASS = MMIN THEN LINE (XVAL, YVAL)-(XVAL, YVAL) ELSE GOTO 1190
1180 RETURN
1190 LINE -(XVAL, YVAL)
1200 RETURN
1210 REM END OF SUBROUTINE****************************************************
1250 END
1500 END
```

Toshiba T1000 PARADAQ execution code

(For use with the Hemond backpack mass spectrometer)

```
1  GOSUB 280
   DIM ARRAY(200)
2  CLS
   PRINT "Mass Spectrometer Control Options"
   PRINT "Select option, then press ENTER"
   PRINT " "
   PRINT "1) DISPLAY SPECTRUM FROM DISK"
   PRINT "2) SCAN"
   PRINT "3) CALIBRATE"
   PRINT "4) EXIT"
   INPUT "OPTION CHOICE?", IX
   IF IX = 1 THEN GOSUB 1250
   IF IX = 2 THEN GOSUB 10
   IF IX = 3 THEN GOSUB 400
   IF IX = 4 THEN END
   GOTO 2
10 REM SCAN OPTION
40 REM DISPLAY/GET PARAMETERS
50 GOSUB 150
60 REM SETUP SCREEN
70 GOSUB 580
105 GOSUB 800
110 RETURN
130 REM END OF MAIN PROGRAM**************************************************
140 REM
150 REM DISPLAY PARAMETERS
160 PRINT "Minimum M/Z", MMIN
170 PRINT "Maximum M/Z", MMAX
180 PRINT "M/Z Step", MSTEP
190 PRINT "Settling Time", STLTIM
200 PRINT "Read Time", RTIME
210 PRINT "Calibrate Slope", CALSLOPE
220 PRINT "Offset", OFFSET
221 IF PLOTTYP$ = "LG" THEN PRINT "Logarithmic Plot"
222 IF PLOTTYP$ = "LN" THEN PRINT "Linear Scale; Scalefactor =", SCLEFACT
230 INPUT "NEW PARAMETERS? (Press N for new parameters, ENTER for scan)",
    YN$

240 IF YN$ = "n" THEN GOSUB 400 ELSE RETURN
250 GOTO 150
260 REM END OF SUBROUTINE****************************************************
270 REM
280 REM INITIALIZE SUBROUTINE
290 MMIN = 12
300 MMAX = 150
310 MSTEP = .5
320 STLTIM = 1
330 RTIME = 1
```

```
340 CALSLOPE = 53.36
350 OFFSET = 0
351 PLOTTYP$ = "LN"
352 SCLEFACT = 14.5
360 RETURN
370 REM END OF SUBROUTINE*****************************************************
380 REM
390 STOP
400 REM PARAMETERS SUBROUTINE
410 INPUT "Minimum M/Z", X
420 IF X > .1 THEN MMIN = X
430 INPUT "Maximum M/Z", X
440 IF X > .1 THEN MMAX = X
450 INPUT "M/Z Step", X
460 IF X > .1 THEN MSTEP = X
470 INPUT "Settling Time", X
480 IF X > .1 THEN STLTIM = X
490 INPUT "Read Time", X
500 IF X > .1 THEN RTIME = X
510 INPUT "Calibration Slope", X
520 IF X > .1 THEN CALSLOPE = X
530 INPUT "Offset", X
REM 540 IF X > .1 THEN OFFSET = X
541 INPUT "Linear (LN) or Logarithmic (LG) Plot Desired?", X$
542 IF X$ = "LN" THEN PLOTTYP$ = "LN" ELSE PLOTTYP$ = "LG"
543 INPUT "Scale Factor for Linear Plot", X
544 IF X > .1 THEN SCLEFACT = X
550 RETURN
560 REM END OF SUBROUTINE*****************************************************
570 REM
580 REM SETUP SCREEN
590 REM TOSHIBA T1000 IS X = 640 PIXELS, Y = 200 PIXELS (EACH LINE/COLUMN
    IS 8)

600 CLS
610 SCREEN 2
620 LINE (32, 8)-(632, 155), , B
630 LOCATE 2, 2
640 PRINT "10"
650 LOCATE 6, 3
660 PRINT "8"
670 LOCATE 10, 3
680 PRINT "6"
690 LOCATE 14, 3
700 PRINT "4"
710 LOCATE 18, 3
720 PRINT "2"
730 LOCATE 21, 3
740 PRINT MMIN
750 LOCATE 21, 76
760 PRINT MMAX
```

```
770 RETURN
780 REM END OF SUBOUTINE*************************************************
790 REM
800 REM SCANNING ROUTINE
810 ERASE ARRAY
820 INDARR = 0
830 REM START OF SCAN LOOP UNTIL MASS >MMAX
850 MASS = MMIN

REM 860 DAVOLTS = CALSLOPE / MASS + OFFSET
REM 870 BITCNT = 6553.5 * DAVOLTS

860 DAVOLTS = 862502.2762188# / (MASS + OFFSET)
870 BITCNT = DAVOLTS - 5746.1838018659#
880 MSB = INT(BITCNT / 256)
890 LSB = INT(BITCNT - MSB * 256)
891 REM OUTPUT TO DA CONVERTER FIRST HIGH, THEN LOW
900 OUT &H37A, 4
901 OUT &H378, MSB
902 OUT &H37A, 0
903 OUT &H37A, 4
904 OUT &H37A, 6
905 OUT &H378, LSB
906 OUT &H37A, 2
907 OUT &H37A, 6
908 OUT &H37A, 4
910 INDARR = INDARR + 1
920 REM DELAY LOOP***********************************************************
930 FOR I = 1 TO STLTIM
940 NEXT I
REM 970 FOR I = 1 TO 5
REM 980 NEXT I
990 GOTO 1020
REM IF LOC(1) > 0 THEN GOTO 1020 ELSE LOCATE 10, 10
991 REM DON'T THINK 990 & 1000 WILL WORK
1000 PRINT "NO RESPONSE FROM INTERFACE"
1010 RETURN
1019 REM INPUT READ FROM AD CONVERTER
1020 OUT &H37A, 165
1021 OUT &H37A, 164
1022 OUT &H37A, 165
1023 hibyte = INP(&H378)
1024 OUT &H37A, 167
1026 lobyte = INP(&H378)
1040 inbits = (hibyte * 256) + (lobyte)
1045 inbytes = INT(inbits)
       IF inbytes > 32767 THEN GOTO 1046 ELSE GOTO 1050
1046 inbolts = (((inbytes - 65536) / 32768) * 5) + 5
      GOTO 1051
1050 inbolts = ((inbytes / 32768) * 5) + 5
1051 involts = inbolts + .002 + ((inbolts / 65536) * .008)
```

```
        LOCATE 21, 40
        PRINT "Digital Word=", inbytes
        LOCATE 22, 40
        PRINT "         mV=", involts * 1000
        LOCATE 21, 15
        PRINT "LOWBYTE =", lobyte
        LOCATE 22, 15
        PRINT "HIGHBYTE=", hibyte
1055 GOTO 1079
1077 REM THIS IS IN VOLTS...EXPECT -5V TO 5V
1078 REM PLOT DATA
1079 GOSUB 1120
1080 MASS = MASS + MSTEP
1081 IF MASS > MMAX THEN GOTO 1082 ELSE GOTO 860
1082 CLOSE
1083 LOCATE 24, 5
1084 INPUT "Type 1 to abandon spectrum file, ENTER to Save ", IY
        IF IY = 1 THEN RETURN
        INPUT "Please type the filename of spectrum file", NAME$
        OPEN NAME$ FOR OUTPUT AS #2
        FOR IZ = 1 TO INDARR
        WRITE #2, ARRAY(IZ)
        NEXT IZ
        REM THE FILE CONTAINS A SPECTRUM WITH EVEN ELEMENTS=MASS
        REM THE FOLLOWING EVEN ELEMENTS=VOLTAGE
1090 RETURN
1100 REM END OF SCAN ROUTINE*****************************************************
1110 REM
1120 REM PLOT SCAN ON SCREEN - MASS VS LOG (INVOLTS * 1000)
1130 XVAL = 32 + 600 * (MASS - MMIN) / (MMAX - MMIN)
1150 IF involts < .001 THEN involts = .001
1151 IF PLOTTYP$ = LG$ THEN GOTO 1160
1152 YVAL = 154 - (involts * SCLEFACT)
1153 GOTO 1170
1160 YVAL = 154 - (LOG(1000 * involts)) * 15.2
1170 IF MASS = MMIN THEN LINE (XVAL, YVAL)-(XVAL, YVAL) ELSE GOTO 1190
1180 RETURN
1190 LINE -(XVAL, YVAL)
1200 RETURN
1210 REM END OF SUBROUTINE*******************************************************
1250 END
1500 END
```

APPENDIX C: Mechanical drawings

Inlet apparatus Ortho cut away view

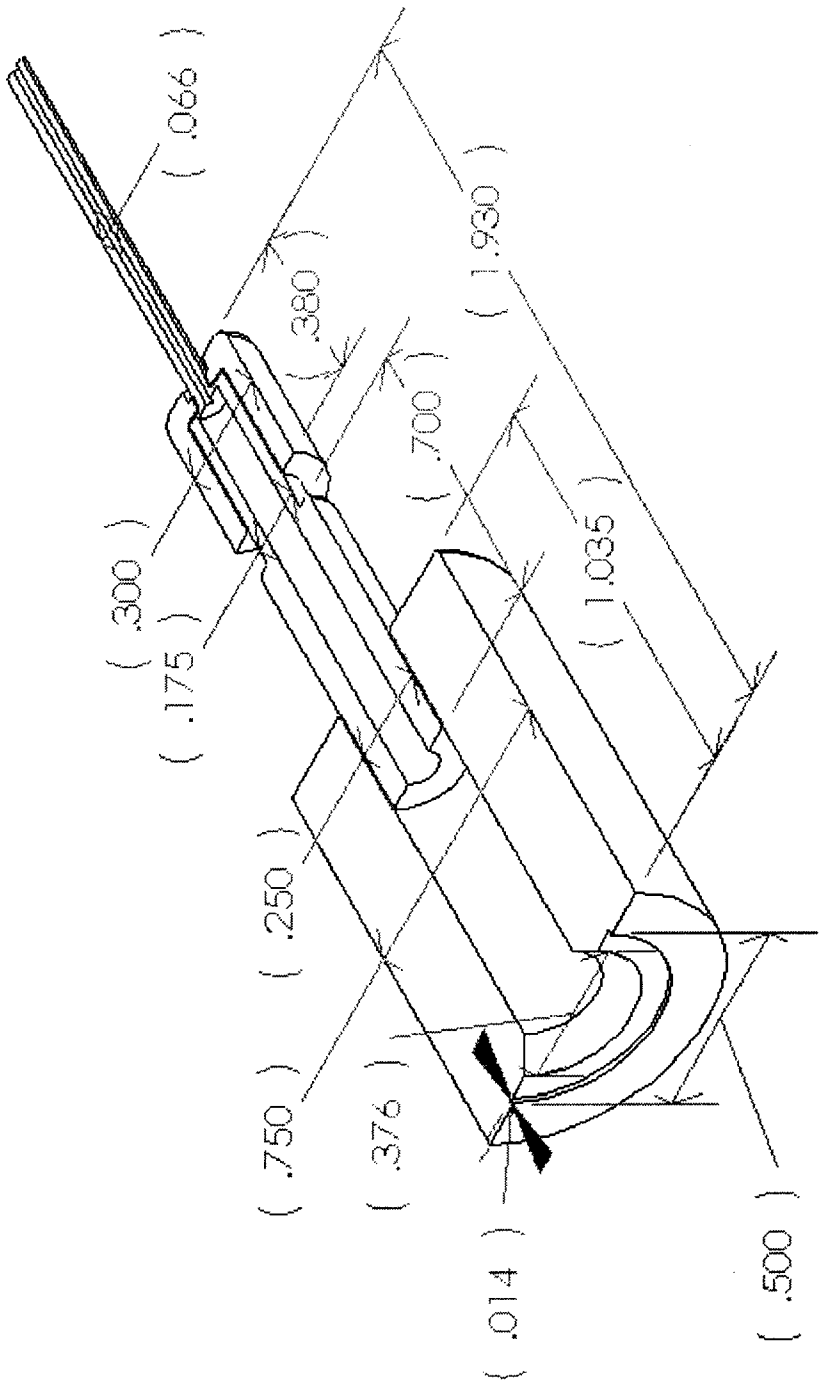

Dimensions in inches

Cycloid heater box Ortho view

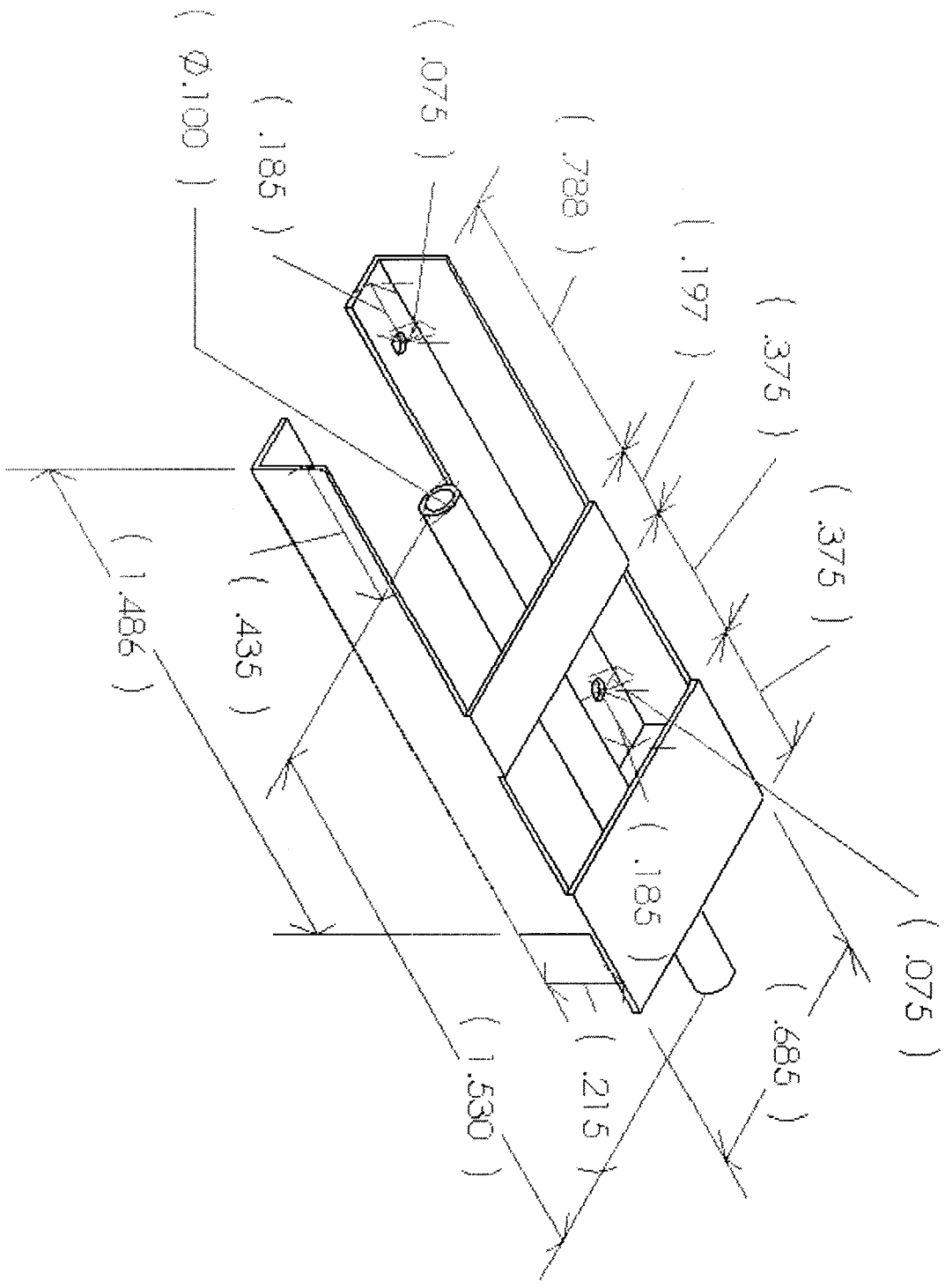

Dimensions in inches

Vacuum envelope Ortho view

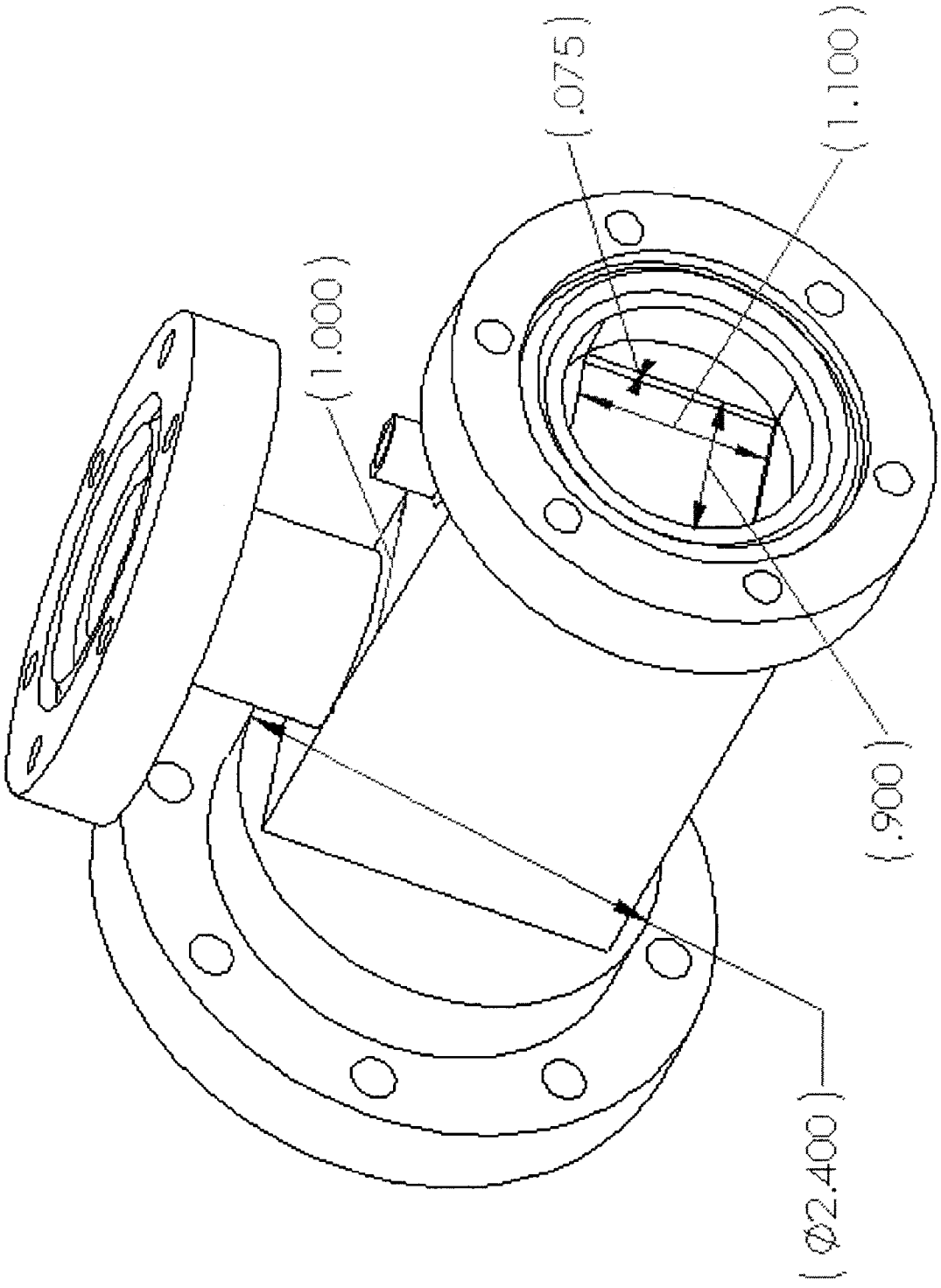

Dimensions in inches

Vacuum envelope Side view

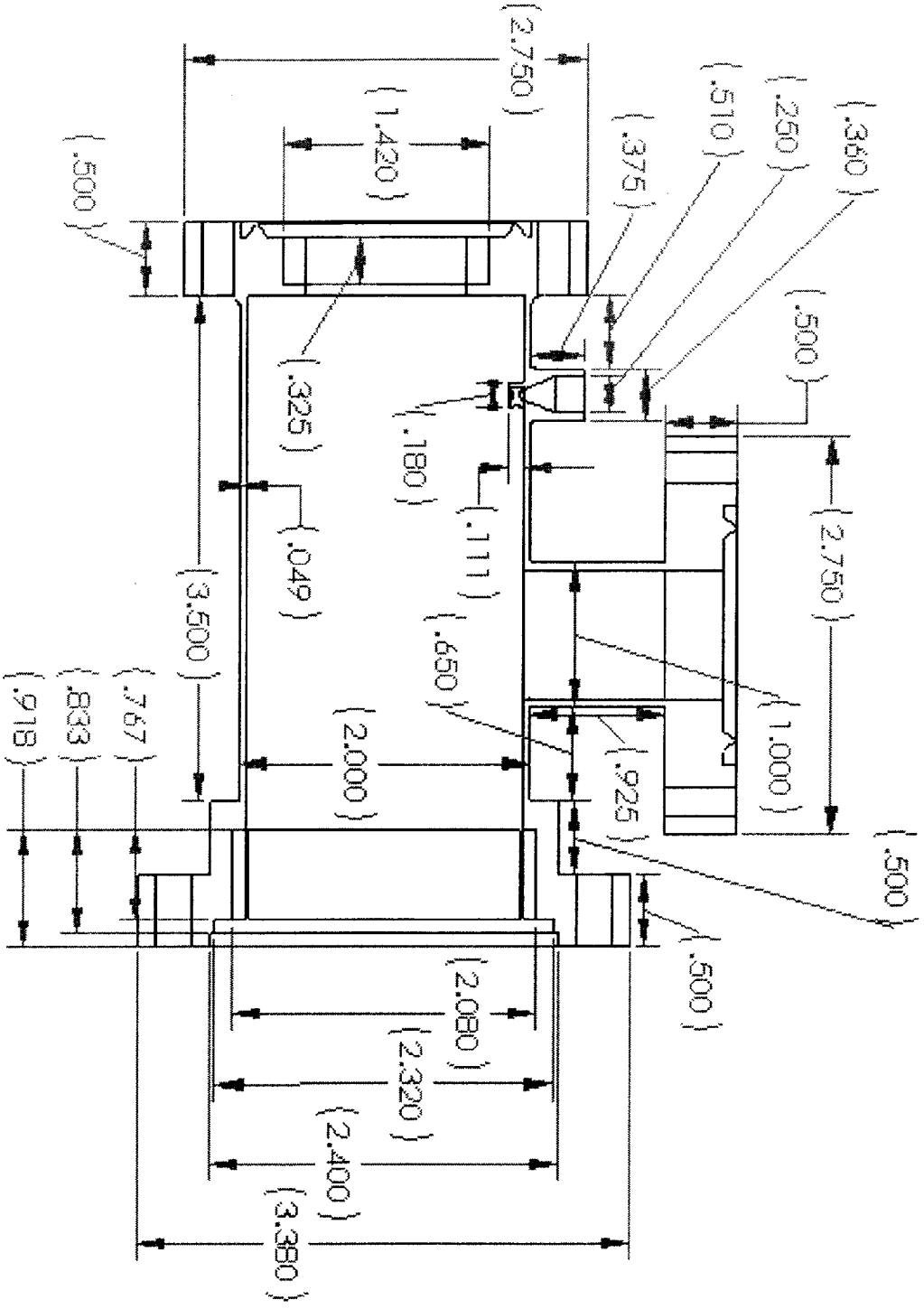

Dimensions in inches

Cycloid magnet Side view

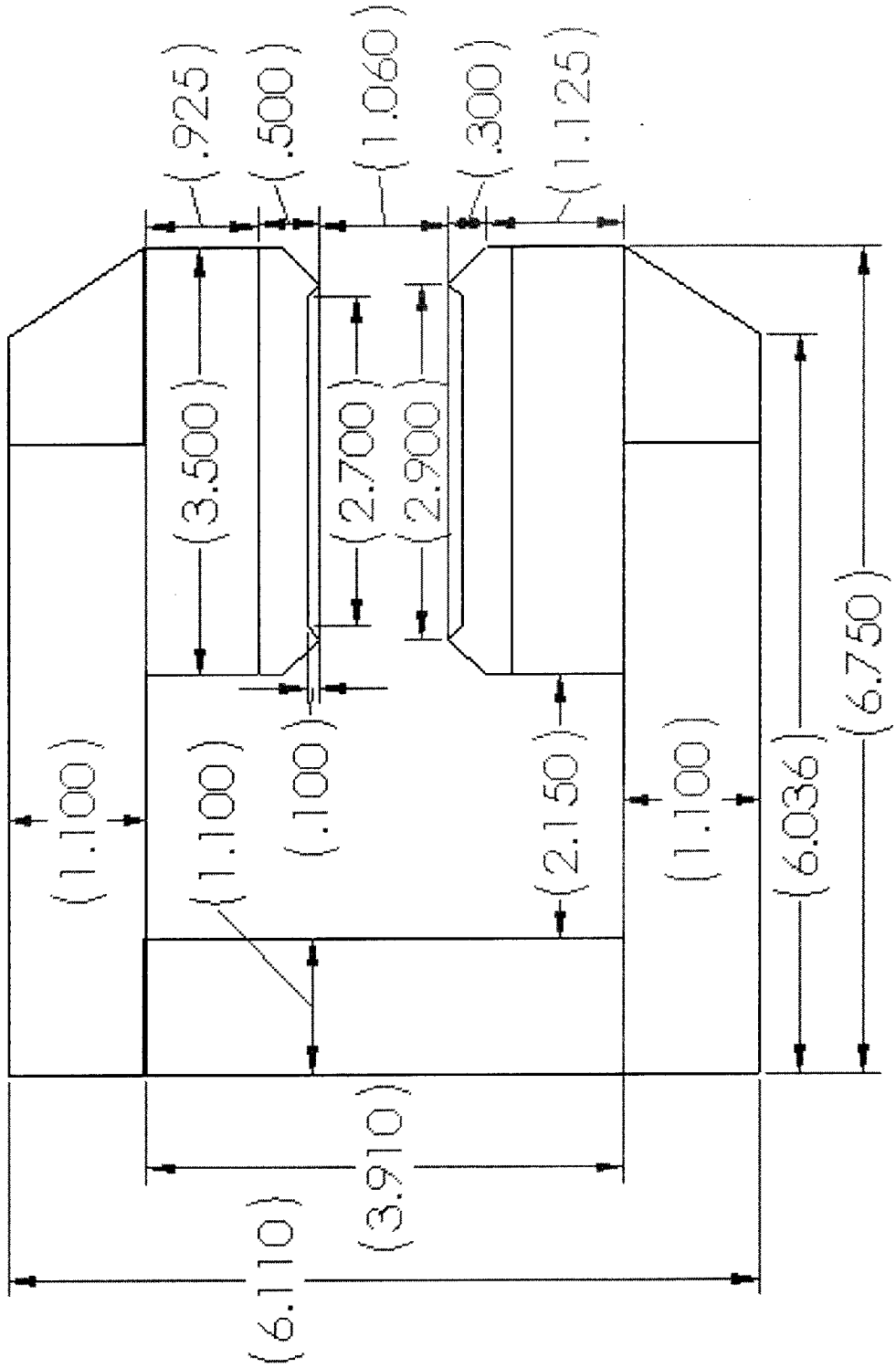

Dimensions in inches

Cycloid magnet Top view

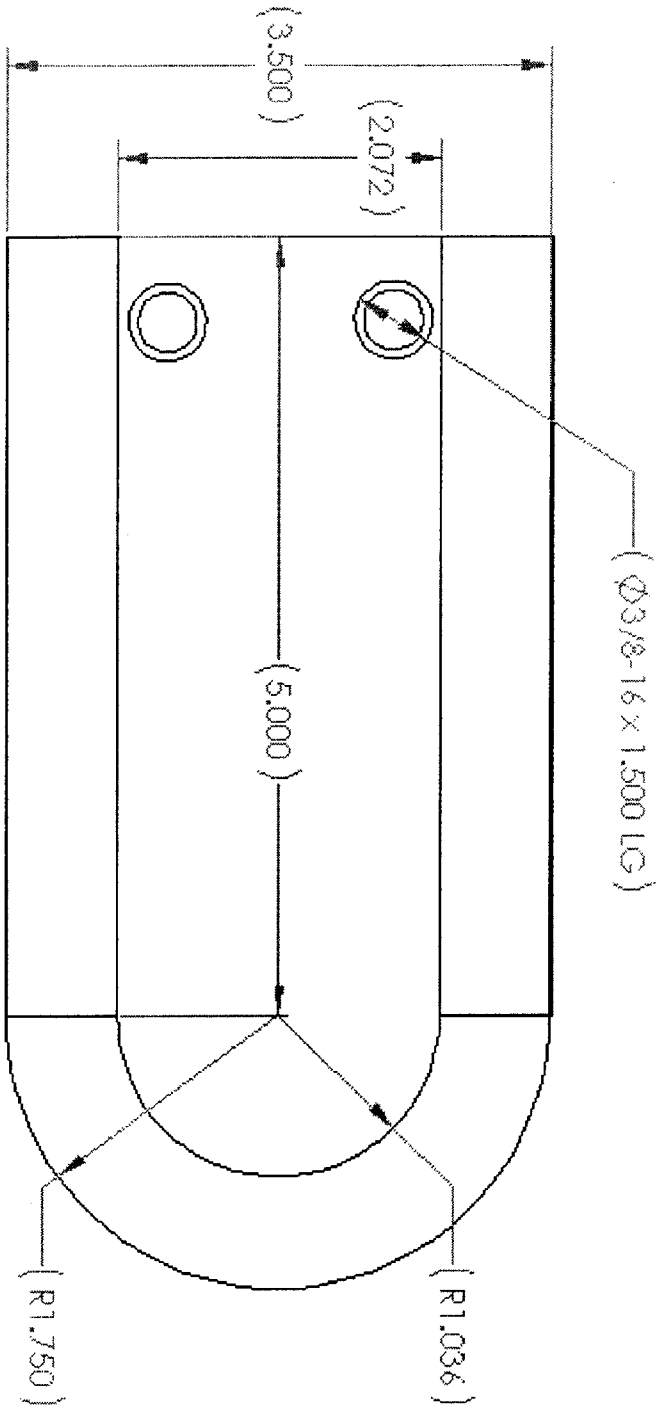

Dimensions in inches

APPENDIX D: Equation derivations & chemical coefficients

Minimum sensitivity determination

Given a minimum sensitivity to argon is 10^{-12} grams/sec, a minimum influx rate of any gas in moles per second, n, can be found. This mass flux can then be easily converted and expressed in terms of cm^3/second @STP, Q.

$$\text{Detection limit}_{Ar} = 10^{-12}\ \frac{\text{grams}}{\text{sec}}$$

$$\downarrow$$

$$n = 2.5 \times 10^{-14}\ \frac{\text{moles}}{\text{sec}}$$

$$\downarrow$$

$$Q = 5.6 \times 10^{-10}\ \frac{cm^3}{\text{sec}}\ @\text{STP}$$

This flux rate, Q, can then be used in conjunction with the permeability constant of the inlet membrane polymer to a given gas, P, the surface area of the permeable polymer, A, the polymer thickness, l, and the partial pressure of the given gas inside the vacuum system, p_1, to determine the partial pressure of the gas on the external surface of the membrane, p_2, that is needed to generate the minimum detectable signal, from (Comyn 1985).

$$Q\left(\frac{cm^3@stp}{\text{sec}}\right) = \frac{P\left(\frac{(cm^3@stp)\cdot cm}{cm^2 \cdot \text{sec} \cdot \text{atm}}\right) A(cm^2)}{l(\text{cm})}\left(p_1(atm) - p_2(atm)\right)$$

The minimum necessary external partial pressure of the gas can then be converted to an equivalent dissolved aquatic concentration via the gas's Henry's constant.

$$[\text{gas}]\left(\frac{\text{moles}}{\text{L}}\right) = p_1(\text{atm}) \times K_H\left(\frac{\text{moles}}{\text{L}\cdot\text{atm}}\right)$$

Permeability coefficients for various gases across inlet membrane[7]

	LDPE ρ= 0.914	HDPE ρ= 0.964
Argon	**2.12×10^{-8}**	**1.31×10^{-8}**
Carbon dioxide	**9.60×10^{-8}**	**2.73×10^{-9}**
Carbon monoxide	**1.11×10^{-8}**	**1.52×10^{-9}**
Ethane	**5.15×10^{-8}**	**4.44×10^{-9}**
Helium	**3.74×10^{-8}**	**8.69×10^{-9}**
Hydrogen	**7.4×10^{-8}**	
Hydrogen sulfide	**2.72×10^{-7}**	
Methane	**2.22×10^{-8}**	**2.93×10^{-9}**
Neon	**4.84×10^{-9}**	
Nitrogen	**7.37×10^{-9}**	**1.11×10^{-9}**
Oxygen	**2.22×10^{-8}**	**3.03×10^{-9}**
Propane	**7.17×10^{-8}**	**4.08×10^{-9}**
Propene	**1.11×10^{-7}**	**8.79×10^{-9}**
Water	**6.87×10^{-7}**	**9.09×10^{-8}**

Permeability values expressed in units of $\left(\frac{(cm^3@stp)\cdot cm}{cm^2 \cdot sec \cdot atm}\right)$ at 25 °C

[7] from(Pauly 1999)

Diffusivity coefficients for various gases across inlet membrane[8]

	LDPE $\rho = 0.914$	HDPE $\rho = 0.964$
Argon	3.60×10^{-7}	1.20×10^{-7}
Carbon dioxide	3.72×10^{-7}	1.20×10^{-7}
Carbon monoxide	3.32×10^{-7}	9.60×10^{-8}
Ethane	6.80×10^{-8}	1.50×10^{-8}
Helium	6.80×10^{-6}	3.07×10^{-6}
Hydrogen	4.74×10^{-7}	
Methane	1.93×10^{-7}	5.70×10^{-8}
Neon	2.42×10^{-6}	
Nitrogen	3.20×10^{-7}	9.30×10^{-8}
Oxygen	4.60×10^{-7}	1.70×10^{-6}
Propane	3.22×10^{-8}	4.90×10^{-9}
Propene	5.80×10^{-8}	1.10×10^{-8}

Diffusivity values expressed in units of cm^2/sec at 25 °C

[8] from (Pauly 1999)

Henry's Law coefficients for various gases in water[9]

Argon	**1.40×10^{-3}**
Carbon dioxide	**3.47×10^{-2}**
Carbon monoxide	**9.50×10^{-4}**
Ethane	**2.00×10^{-3}**
Helium	**3.80×10^{-4}**
Hydrogen	**7.94×10^{-4}**
Methane	**1.29×10^{-3}**
Neon	**4.50×10^{-4}**
Nitrogen	**6.60×10^{-4}**
Oxygen	**1.26×10^{-3}**
Propane	**1.50×10^{-3}**
Propene	**4.80×10^{-3}**

Henry's constant values expressed in units of mol/(L·atm) at 25 °C

[9] from (Sander 1999)

Conductance determinations for vacuum system components

Formulae for conductance of gases[10]

A = area (cm^2)
F = conductance (cm^3/sec)
H = height (cm)
K = proportionality constant (unitless)
L = length (cm)
M = molecular weight (grams/mol)
P = pressure (atm)
Q = volumetric flux rate (cm^3/sec @stp)
T = temperature (Kelvin)
τ = residence time (sec)

Through a long circular tube:

$$F = 3638 \times K \times A \times \left(\frac{T}{M}\right)^{1/2}$$

Through a rectangular tube:

$$F = \frac{3.638 \times A \times \left(\frac{T}{M}\right)^{1/2}}{1 + \frac{3}{16} \times \left(\frac{H \times L}{A}\right)}$$

Conductance of water vapor within vacuum system components at 5 °C

	K	(l/sec)	(cm^3/sec)
pump inlet	5.14E-01	2.84E+01	2.84E+04
ion pump	4.53E-01	4.10E+01	4.10E+04
vac env		2.35E+00	2.35E+03
inlet tube	2.66E-03	2.87E-03	2.87E+00
overall		2.86E-03	2.86E+00

Membrane Inlet
⇓
Inlet Tube
⇓
Vacuum Envelope
⇓
Pump Inlet
⇓
Ion Pump

Water vapor residence time in inlet tube:

$$\tau = \frac{\text{Volume}\,(cm^3)}{F\left(\frac{cm^3}{sec}\right)} = \frac{L \times A}{F}$$

Flow rate & pressure difference of water vapor in inlet tube:

$$P2 - P1 = \frac{Q}{F}$$

[10]From Scientific Foundations of Vacuum Technique, Duschman, pp. 93-97

Vacuum envelope steady state pressure determination

Given a constant vacuum envelope internal volume, and assuming steady state internal pressure and temperature conditions, the condition of mass in (gas influx) equaling mass out (gas sequestered by the ion pump) must be satisfied.

$$\text{Mass}_{\text{in}} = \text{Mass}_{\text{out}}$$

Water vapor is expected to dominate the mass influx into the vacuum system. Therefore, using the permeability coefficient of the inlet membrane to water (P), the surface area of the permeable polymer (A), the polymer thickness (l), and assuming the partial pressure of water vapor inside the vacuum system (p_2) is negligible, and that the partial pressure of water vapor on the external surface of the membrane is a function of temperature (p_1), a water vapor influx rate can be estimated.

$$Q\left(\frac{\text{cm}^3\text{@stp}}{\text{sec}}\right) = \frac{P\left(\frac{(\text{cm}^3\text{@stp})\cdot\text{cm}}{\text{cm}^2\cdot\text{sec}\cdot\text{atm}}\right) A(\text{cm}^2)}{l(\text{cm})}\left(p_1(atm) - p_2(atm)\right)$$

This influx rate, Q, can alternately be expressed in terms of L·atm/sec by multiplying by a conversion factor of 10^{-3} L/cm^3, assuming temperature near 273K. From mass balance, this influx must equal water vapor uptake by the pump, which is the product of steady state pressure and the limiting conductance of the vacuum system. Steady state pressure, p_{ss} (atm), can thus be estimated by dividing this flux rate, Q (L·atm/sec), by the vacuum envelope conductance, F (L/sec).

$$p_{ss}(\text{atm}) = \frac{Q\left(\frac{\text{L}\cdot\text{atm}}{\text{sec}}\right)}{F\left(\frac{\text{L}}{\text{sec}}\right)}$$

Tables of inlet backing plate depth limits using various design specifications

Backing plate maximum depth limit (in feet) as a function of unsupported aperture radius (in inches) and plate thickness (in inches):

Simply held #304 stainless steel plate with 21% void

					Plate	thickness				
radius	0.01	0.014	0.025	0.05	0.075	0.1	0.125	0.15	0.175	0.2
0.1	588	1,186	4,845	15,524	34,970	62,196	97,200	139,983	190,545	248,885
0.125	364	747	3,089	9,923	22,369	39,793	62,196	89,577	121,936	159,274
0.15	243	508	2,134	6,881	15,524	27,624	43,181	62,196	84,668	110,597
0.175	169	364	1,559	5,046	11,396	20,286	31,716	45,686	62,196	81,246
0.1875	143	313	1,354	4,391	9,923	17,667	27,624	39,793	54,175	70,770
0.2	122	271	1,186	3,855	8,717	15,524	24,275	34,970	47,611	62,196
0.225	89	207	930	3,039	6,881	12,258	19,173	27,624	37,611	49,135
0.25	66	161	747	2,455	5,567	9,923	15,524	22,369	30,459	39,793
0.275	48	127	611	2,023	4,595	8,195	12,824	18,481	25,167	32,881
0.3	35	102	508	1,695	3,855	6,881	10,770	15,524	21,142	27,624
0.325	25	82	428	1,439	3,280	5,858	9,172	13,222	18,009	23,532
0.35	17	66	364	1,236	2,824	5,046	7,904	11,396	15,524	20,286
0.375	10	53	313	1,072	2,455	4,391	6,881	9,923	13,518	17,667
0.4	5	42	271	938	2,154	3,855	6,043	8,717	11,877	15,524

Simply held #304 stainless steel plate with 31% void [11]

					Plate	thickness				
radius	0.005	0.01	0.02	0.03	0.04	0.05	0.06	0.07	0.08	0.09
0.1	102	510	2,140	4,858	8,663	13,554	19,533	26,599	34,752	43,992
0.125	53	314	1,358	3,097	5,532	8,663	12,489	17,011	22,229	28,142
0.15	27	208	932	2,140	3,831	6,005	8,663	11,803	15,426	19,533
0.175	10	144	676	1,563	2,806	4,403	6,355	8,663	11,325	14,342
0.1875	5	121	585	1,358	2,440	3,831	5,532	7,542	9,861	12,489
0.2	0	102	510	1,189	2,140	3,363	4,858	6,624	8,663	10,973
0.225	-7	73	396	932	1,684	2,650	3,831	5,227	6,837	8,663
0.25	-12	53	314	749	1,358	2,140	3,097	4,227	5,532	7,010
0.275	-16	38	254	613	1,116	1,763	2,553	3,488	4,566	5,788
0.3	-19	27	208	510	932	1,476	2,140	2,925	3,831	4,858
0.325	-21	18	172	429	789	1,253	1,819	2,488	3,259	4,134
0.35	-23	10	144	365	676	1,075	1,563	2,140	2,806	3,560
0.375	-24	5	121	314	585	932	1,358	1,860	2,440	3,097
0.4	-25	0	102	272	510	815	1,189	1,631	2,140	2,718

[11] negative depth values are due to the included pressure difference of 1 atmosphere

Table of inlet membrane depth limits using various design specifications

Inlet membrane maximum depth limit (in feet) as a function of backing plate hole radius (in inches) and membrane thickness (in inches):

Low density polyethylene $\rho = 0.914$

	Membrane thickness											
radius	0.0005	0.0010	0.0015	0.0020	0.0025	0.0030	0.0035	0.0040	0.0045	0.0050	0.0055	0.0060
0.0010	1539	3112	4686	6259	7832	9405	10978	12552	14125	15698	17271	18844
0.0015	1015	2064	3112	4161	5210	6259	7308	8356	9405	10454	11503	12552
0.0020	753	1539	2326	3112	3899	4686	5472	6259	7045	7832	8619	9405
0.0025	595	1225	1854	2483	3112	3742	4371	5000	5630	6259	6888	7517
0.0030	491	1015	1539	2064	2588	3112	3637	4161	4686	5210	5734	6259
0.0035	416	865	1315	1764	2214	2663	3112	3562	4011	4461	4910	5360
0.0040	359	753	1146	1539	1933	2326	2719	3112	3506	3899	4292	4686
0.0045	316	665	1015	1364	1714	2064	2413	2763	3112	3462	3812	4161
0.0050	281	595	910	1225	1539	1854	2169	2483	2798	3112	3427	3742
0.0055	252	538	824	1110	1396	1682	1968	2254	2540	2826	3112	3398
0.0060	228	491	753	1015	1277	1539	1801	2064	2326	2588	2850	3112
0.0065	208	450	692	934	1176	1418	1660	1902	2144	2386	2628	2870
0.0070	191	416	640	865	1090	1315	1539	1764	1989	2214	2438	2663
0.0075	176	386	595	805	1015	1225	1434	1644	1854	2064	2273	2483
0.0080	163	359	556	753	949	1146	1343	1539	1736	1933	2129	2326
0.0085	151	336	521	706	892	1077	1262	1447	1632	1817	2002	2187
0.0090	141	316	491	665	840	1015	1190	1364	1539	1714	1889	2064
0.0095	132	297	463	628	794	960	1125	1291	1456	1622	1788	1953
0.0100	123	281	438	595	753	910	1067	1225	1382	1539	1697	1854